FUNCTIONALIZATION OF INHALABLE PARTICLES BY FLUIDIZED BED PROCESSING

by

Teófilo Donaires Flores

A thesis submitted in partial fulfillment of the requirements for the degree of

MASTER OF SCIENCE
in
CHEMICAL ENGINEERING

UNIVERSITY OF PUERTO RICO
MAYAGÜEZ CAMPUS
2008

Approved by:

_____	_____
Guillermo Colón, Ph.D. Member, Graduate Committee	Date
_____	_____
L. Antonio Estévez, Ph.D. Member, Graduate Committee	Date
_____	_____
Carlos Velázquez, Ph.D. President, Graduate Committee	Date
_____	_____
Rodolfo Romañach, Ph.D. Representative of Graduate Studies	Date
_____	_____
David Suleiman, Ph.D. Chairperson of the Department	Date

ABSTRACT

This work focused initially on the size reduction of naproxen sodium to less than 5 μm for inhalation applications. The second objective was the adhesion of naproxen sodium particles to micronized lactose particles with an average size below 5 μm. Both processes were executed in a fluid bed processing unit at high vacuum pressure.

The desired particles were obtained by precipitation in a fluid bed processing unit at a pressure at the nozzle of 551.43 kPa from a naproxen sodium solution flowing at 1.0 ml/s for 30 seconds through a nozzle. This solution contained 30% (v/v) ethanol, 20% naproxen sodium by weight at a temperature of 313.15 K. The solution entered the fluid bed processing unit operating at high vacuum pressure which maintains the fluidization with a flow rate of air at 5 m/s for 10 minutes. These conditions ensured a crystallization of naproxen sodium smaller than 5 μm.

The functionalization of the particles of the micronized lactose particles by naproxen sodium were performed in the same fluid bed processing unit under the same conditions used for the crystallization process of naproxen sodium.

The composition of the particles functionalized was determined using Energy Dispersive X-Ray microanalysis, which identified the sodium atoms of the crystallized naproxen sodium.

The crystalline structure of micronized lactose, naproxen sodium, naproxen sodium crystallized, and particles functionalized was determined using X-Ray Diffraction with Kα

1.54056 A° with a range angle of 7° to 74° showing a small deviation between micronized lactose and naproxen sodium crystallized. It is shown that a change in the crystal arrangements between naproxen sodium and naproxen sodium crystallized occurred after the crystallization.

The average particles size obtained for the micronized lactose was 2.349 µm, for the naproxen sodium crystallized is 2.280 µm, and for the particle functionalized is 4.040 µm. The images of the particles obtained with a Scanning Electron Microscope were analyzed with the Scandium Software for the determination of particle sizes, and morphology. The accumulation distribution of the micronized lactose particles and naproxen sodium crystallized with less than 5 µm was 90%, and 80% for the particles functionalized.

The micronized lactose, naproxen sodium, naproxen sodium crystallized, and particles functionalized were characterized using Fourier Transform Infrared Spectroscopy. The wavenumber region studied for the particles functionalized was from 960 – 1160 cm^{-1}. However, the wavenumber range for the micronized lactose, naproxen sodium, and naproxen sodium crystallized was 780 – 1680 cm^{-1}.

The particles functionalized resulted by adhesion of naproxen sodium crystallized over micronized lactose were due to Van der Waals, intermolecular, electrostatic, and magnetic forces. These particles functionalized can be used as inhalation products since they complied with the requirement of a particle size less than 10 µm.

RESUMEN

El presente trabajo se enfocó inicialmente en la reducción del tamaño de partículas de naproxeno sódico a menos de 5 µm para aplicación en productos de inhalación. El segundo objetivo es adherir las partículas de naproxeno sódico a las partículas de lactosa micronizada con tamaños debajo de los 5 µm. Los dos procesos se ejecutan en lecho fluidizado a presión de vacío.

Los tamaños de partícula deseados fueron obtenidos por precipitación en un lecho fluidizado a una presión de 551.43 kPa al fluir a través de un pistilo una solución de naproxeno sódico con un flujo de 1.0 ml/s durante 30 s. Esta solución contiene 30% v/v etanol, 20% w/w naproxeno sódico a una temperatura de 313.15 K en lecho fluidizado a presión de vacío manteniendo la velocidad de fluidización a 5 m/s durante 10 minutos para obtener partículas de naproxeno sódico cristalizado menores de 5 µm.

Las partículas funcionalizadas de naproxeno sódico cristalizado sobre lactosa micronizada en lecho fluidizado a presión de vacío se desarrolló con los parámetros y condiciones de operación similar que en el proceso de cristalización de naproxeno sódico.

La composición de las partículas funcionalizadas se determina usando microanálisis dispersivo de la radiografía energética, que identifica los átomos de sodio por el uso de naproxeno sódico cristalizado en la funcionalización.

La estructura cristalina de naproxeno sódico cristalizado, naproxeno sódico ,lactosa micronizada y las partículas funcionalizada se han determinado usando la Difracción de Rayos X con Kα 1.54056 A° y un rango de ángulo de 7 – 47°, mostrando ligeros cambios en

la estructura cristalina entre la lactosa micronizada y naproxeno sódico cristalizado. Se puede observar un cambio en los arreglos cristalinos entre naproxeno sódico y naproxeno sódico cristalizado que ocurren como resultado de la cristalización.

El promedio del tamaño de partículas de lactosa micronizada es de 2.349 µm, para naproxeno sódico cristalizado es 2.280 µm y para las partículas funcionalizadas es de 4.040 µm. El tamaño de partículas y su morfología fueron determinados a través de imágenes tomadas con el microscopio electrónico de barrido y analizados con la aplicación *Scandium*. La distribución de la acumulación de tamaño de partículas de lactosa micronizada y naproxeno sódico cristalizado de las partículas que son menores de 5 µm es de 90% y la partículas funcionalizadas es 80%.

Los grupos funcionales de lactosa micronizada, naproxeno sódico y naproxeno sódico cristalizado se han determinado usando espectroscopia de Transformada de Fourier Infra Rojo, en el rango 780 – 1680 cm^{-1} de longitud de onda. El rango obtenido para las partículas funcionalizadas es 960 – 1160 cm^{-1}.

Las partículas funcionalizadas resultan de la adhesión de naproxeno sódico cristalizado sobre lactosa micronizada debido a las fuerzas de Van der Waals, fuerzas intermoleculares, fuerzas electrostáticas y fuerzas magnéticas.

Las partículas funcionalizadas se pueden utilizar como partículas de inhalación debido a que cumplen con los requisitos de tamaño menores de 10 µm.

To GOD

To the memory of my father and brothers

To my love Susy

To my children Karol Konrad and Alvaro Jesús

To mother Benedicta

ACKNOWLEDGEMENTS

During the development of my graduate studies in the University of Puerto Rico in the Department of Chemical Engineering several persons and institutions collaborated directly and indirectly with my research. Without their support it would have been impossible for me to finish my work.

I want to start expressing a sincere acknowledgement to my advisor, Dr. Carlos Velázquez Figueroa because he gave me the opportunity to research under his guidance and supervision. I received motivation; encouragement and support from him during all my studies. With him, I have learned to write papers for conferences and sharing my ideas to the public. In addition, I want to thank the example, motivation, inspiration and support that I received from Dr. L. Antonio Estévez De Vidts, and Dr. Guillermo Colón Burgos, to my friends Carmen Villanueva Armán, and Dr. Alvaro Realpe Jiménez, I am completely grateful. Special thanks to Jorge Reyes of IEP for the support in the communication effort with Perú.

The Grant from "Instituto de Estudios Peruanos – IEP" Ford Foundation, and Universidad Nacional del Altiplano, Puno, Perú provided the economical support. At last, but not at least, the most important thanks go to my family, for their unconditional support, inspiration, and love, specially my wife Susy, my mother Benedicta, my children Karol Konrad, and Alvaro Jesús, my brothers, sisters, my father-in-law Pablo, my mother-in-law Angela, and to my brothers and sisters-in-law.

Finally, my best thank of all goes to God, who has always been there for me, and for giving me the chance to achieve all that I have achieved and to be all that I am.

Table of Contents

List of Tables

List of Figures

1 INTRODUCTION

1.1 Motivation

Currently 210 million people have pulmonary chronic obstructive illnesses, and 3 million people died in 2005 due to these illnesses. The World Health Organization (2007) predicts that on the year 2030 these illnesses will become the fourth cause of death. Asthma deaths will increase by almost 20% in the next 10 years if urgent action is not taken [1].

Bronchial asthma and chronic bronchial illnesses are quite frequent. These illnesses are caused mostly by the contamination of the environment. Lung diseases are derived from these illnesses. These lungs diseases exist among all the world population. The most common characteristic is the limitation of the air flow. It is not completely irreversible and it causes the abnormalities in the pulmonary pathways.

The inhalation treatment is administered fundamentally using pressurized metered dose inhalers. These metered inhalers account for eighty percent of the total inhalers, while the other twenty percent use dry powders. One of the inhalers' advantages is that they act naturally as a filter, making it easy for the particles to go into the deep air flow passages of the lungs, and unblock them. The result is a high concentration of active ingredient in the air pathways [2, 3].

Currently there are a lot of problems in the elaboration of inhalers for asthma and bronchial ailments. These problems are related to the dispersion mechanisms, and inadequate particles sizes, and morphology. The use of fluidized bed is suitable since better heat and mass transfer coefficients are obtained.

1.2 Justification

The international opinion agrees that the chronic respiratory diseases should be treated with inhalers. The treatment of these diseases with inhalers has clear advantages to the pulmonary system. It targets great concentration in the pulmonary tracks, which speeds up the process. It diminishes the secondary effects that occur when they are administered orally [1].

Nowadays the need of technology to obtain submicron particles is growing especially for powder inhalers. The area in much need is product for pulmonary treatment. Figure 1.1 summarizes the current two approaches to treat chronic respiratory diseases and the technology used in the inhalers area.

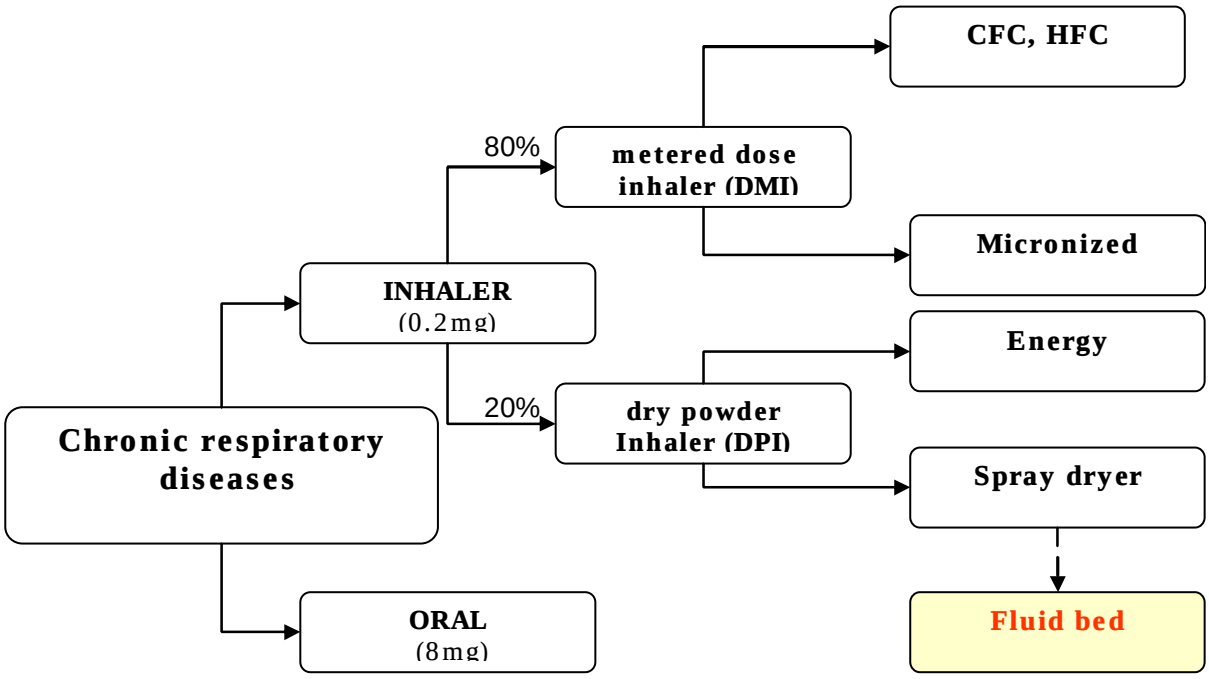

Figure 1.1 The medication manufacture chronic respiratory diseases

As can be seen spray drying has been a technology utilized in the preparation of dry powders, thus it poses fluid bed processing unit as a possible technology to obtain the required powders.

This work focused in the functionalization of submicron lactose with naproxen sodium (NS) using a fluid bed processing unit (FBPU) as an alternative to adhere an active ingredient over a carrier for inhalation treatment.

The most important property related to the inhalers is the size of the particles because this property governs the aerodynamics of the particles in the respiratory tract. As can be seen in Figure 1.1, respiratory illnesses are currently being treated with two types of administration: inhalation, and orally. The inhalation treatment is further divided in two different mechanisms: eighty percent are manufactured as metered dose inhalers (MDI),

which are divided in two types of elaboration: pressurized inhalers with chlorofluorocarbon (CFC), hydro fluorocarbon (HFC), and as micronized particles. The other twenty percent use dry powders (DPI), which are manufactured mainly through spray dryers. These dry powders require energy to disperse the particle in the respiratory tract. The spray dryer method is performed by evaporating the solvent or extracting and condensing the solvent. The pressurized inhalers are not longer manufactured due to environmental concerns regarding CFCs, and HFC. In addition, a therapeutic failure was observed caused by the effect of cold freon, thus it was difficult to administer it.

Historically, the primary ingredients used for with inhalers are obtained by micronization. Unfortunately micronized particles based inhalers had problems with the lack of effective control over the particle size, morphology, and shape. On the micronized particle process, when the particles are broken up they produce particle interactions which increase the electrostatic forces and cohesiveness.

The spray dryer technology is more reliable, and reproducible, because better control can be exercise over the particle size. However, a new alternative, fluid bed processing unit is being considered as a manufacturing technology for dry powder inhalers.

The operational parameters on a fluid bed dryer can be determined and they can be maintained under control. This new technology has advantages because it will eliminate the difficulties in coordination between pulsation and inspiration. The new technology will have a better control in the doses availability, and it will not produce alveolar inhalation.

Figure 1.2 shows the important physical-chemical characteristics in the formulation of dry powder inhaler are the particle sizes, morphology, density, and chemical composition.

The particle size has to be integrated during the development of the pharmaceutical aerosols. The optimal size interval is between 1 and 5 μm. The aerosol particles with sizes above 10 μm have an aerodynamic tendency to impact the mouth and the pharynx, and not enter the lung area. The particles that is smaller, inferior to 5 μm tend to sediment in the smaller pathways, settle in the smallest air roads, which are the terminal bronchi, channels and alveolar sacks where the active principle exercises its therapeutic effect. Particles below 1 μm are generally affected by the Brownian movement and are eliminated during the expiration. In addition since the particles have excessively small diameters, they do not deposit on the lung area [2, 3].

The morphology structure of particles such as surface, texture and porosity have great influence in how the particles interact. The shape of a particle and its geometry is important for latter dispersion of powders. The spherical particles tend to disperse in a normal distribution pattern. However, the straight and extended particles tend to disperse less than spherical particles. The excipients which have smooth and polished surfaces produced optimal results in the flow dispersion.

The powder formulation is obtained by mixing the active ingredient and an auxiliary excipient. In regards to the excipients used in the formulation, the most popular is lactose monohydrate. Other excipients that are used as aides for the flow are fructose, galactose, glucose, manitol, dextrose, and cyclodextrine [2, 3, 6].

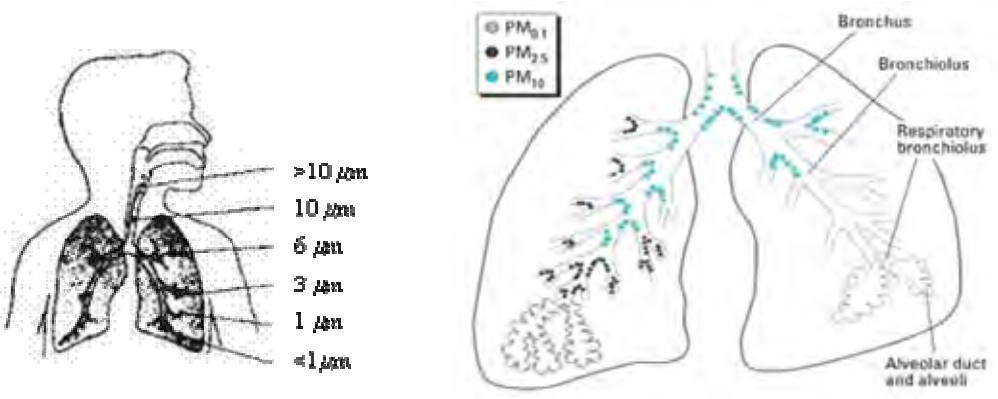

Figure 1.2 Mechanics of inhalation in human of size particle [2]

1.3 Objective

1.3.1 General objective

- To functionalize particles of micronized lactose with naproxen sodium crystallized over its surface in a fluid bed processing unit at high vacuum.

1.3.2 Specifics objectives

- Determine operating conditions to crystallize naproxen sodium in the fluid bed processing unit with sizes less than 5 µm.
- Understand the crystallization process of naproxen sodium over micronized lactose in the fluid bed processing unit.
- Determine physical and chemical properties of the raw material including micronized lactose, and naproxen sodium; and the processed material including naproxen sodium crystallized, and the particle functionalized using Scanning Electron Microscope (SEM), Energy Dispersive X-ray Microanalysis (EDAX), Fourier Transform Infrared (FTIR) spectroscopy, and X-Ray Diffraction (XRD).

2 BACKGROUND AND LITERATURE REVIEW

2.1 Fluidization

Fluidization is a process of physical transformation when an external force is applied, where mainly the solid particles imitate the properties of a fluid, while it increases the distance between particles [5]. The main benefit of this process is the increase of the mass transfer and heat transfer. The main reason is that it centered in the chemical applications, food and pharmaceutical industry [5, 17, 18].

The cohesion parameter plays an important role in the prediction of dynamic behavior in fluidized beds. Although new technology is helping to understand and give more precise prediction in fluidization, more research is still needed [21, 22, 23].

Other important properties are that the fluidized bed has constant temperature, and velocity air flow. An abrupt change in the fluidization speed can be controlled much easier, and because a homogenous distribution exists the temperature implies that all fluidized bed is being processed in the same manner [2, 3].

The particles that pertain to the C group of Geldart classification [24, 25, 27, 42, 43] are very fine powders, and cohesive. Their sizes are usually less than 30 μm, and they are extremely difficult to fluidize because inter-particle forces are relatively large, compared to

those resulting from the action of gas. In small diameter beds, group C particles easily give rise to channeling [5, 43].

2.1.1 Geldart's Classic Classification of Powders

The behavior of solid particles in fluidized beds depends mostly on their size and density. A careful observation by Geldart [24, 25, 27, 42, 43] is depicted in Figure 2.3 in which the characteristics of the four different powder types were categorized as follows:

Group A is designated as aero stable particles. These materials have small mean particle size (d_p < 30 μm) and/or low particle density (<~1.4 g/cm^3). Fluid cracking catalysts typically are in this category. These solids fluidize easily, with smooth fluidization at low gas velocities without the formation of bubbles. At higher gas velocity, a point is eventually reached when bubbles start to form and the minimum bubbling velocity, U_{mb} is always greater than U_{mf}[5, 24].

Group B is called sand like particles and some call it bubbly particles. Most particles of this group have size 150 μm to 500 μm and density from 1.4 to 4 g/cm^3. For these particles, once the minimum fluidization velocity is exceeded, the excess gas appears in the form of bubbles. Bubbles in a bed of group B particles can grow to a large size. Typically used group B materials are glass beads and coarse sand [5, 24].

Group C materials are cohesive or very fine powders. Their sizes are usually less than 30 μm, and they are extremely difficult to fluidize because inter-particle forces are relatively large, compared to those resulting from the action of gas. In small diameter beds, group C

particles easily give rise to channeling. Examples of group C materials are talc, flour and starch [5, 24].

Group D is called spoutable and the materials are either very large or very dense. They are difficult to fluidize in deep beds. Unlike group B particles, as velocity increases, a jet can be formed in the bed and material may then be blown out with the jet in a spouting motion. If the gas distribution is uneven, spouting behavior and severe channeling can be expected. Roasting coffee beans, lead shot and some roasting metal ores are examples of group D materials [5, 24].

Geldart's classification is clear and easy to use as displayed in Figure 2.3 for fluidization at ambient conditions and for U less than about $10 \cdot U_{mf}$. For any solid of a known density ρ_s and mean particle size d_p this graph shows the type of fluidization to be expected. It also helps predicting other properties such as bubble size, bubble velocity, the existence of slugs etc.

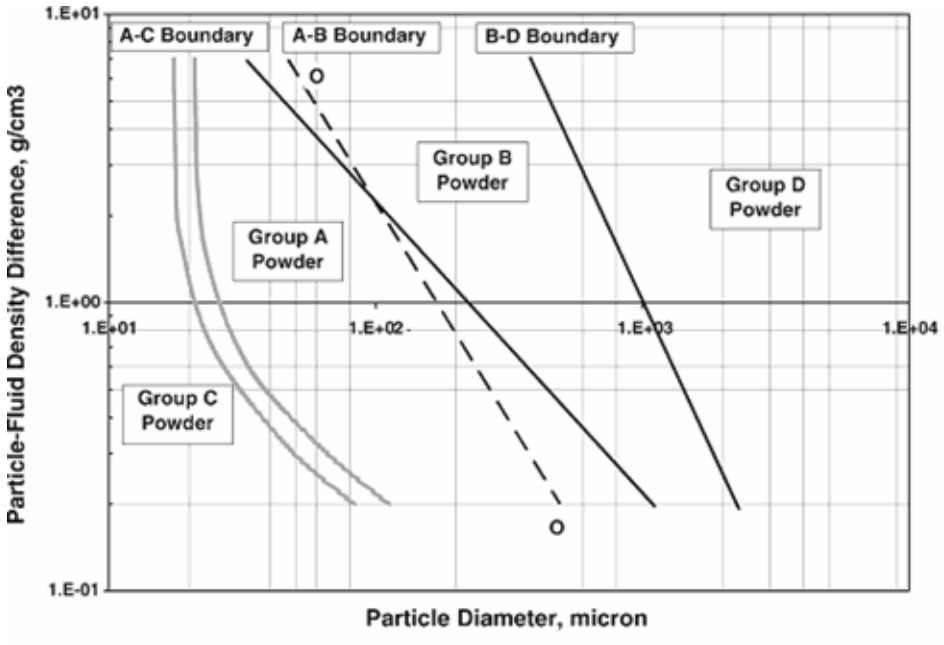

Figure 2.1 Diagram of the Geldart classification [24]

The powders can be classified regarding their properties and their functionality. Geldart's works [24] shows that, for the fluidization process, powders can be classified into four groups Figure 2.3. The according to fluid density, and particles sizes. For example, powders from group C are cohesive and difficult to fluidized, while powders of group A present the aeration property required for coating purposes. Other classification systems, based on the flow regime, are mentioned by Geldart [24].

2.1.2 Phenomenon of Fluidization

If a fluid is passed upward through a bed of fine particles, as shown in Figure 2.1, at a low flow rate, the fluid merely percolates through the void spaces between stationary particles. This is known as fixed bed. With an increase in flow rate, particles move apart and a few vibrate and move in restricted regions. This is known as expanded bed.

Generally, gas-solid systems behave quite differently. With an increase in flow rate beyond minimum fluidization, large instabilities with bubbling and channeling of gas are observed [5, 16, 17].

If the upward flow rate is very large, the bed mobilizes pneumatically and may be swept out of the process chamber. At an intermediate flow rate though the bed expands in what we call an expanded state. In the expanded bed the particles have a free distance between particles and the particles are supported by the drag force of the fluid. The expanded bed has some of the properties of a fluid called a fluidized bed [16,17].

Figure 2.1a shows what happens the occurs when the approach velocity, V_o, is much smaller than the minimized fluidization velocity, V_{om}.

Figure 2.1b shows the behavior when the approach velocity is much greater than the particle terminal velocity, u_f, and the expanded bed.

Figure 2.1c shows behavior when the approach velocity is intermediate between the minimum fluidization velocity and the terminal velocity.

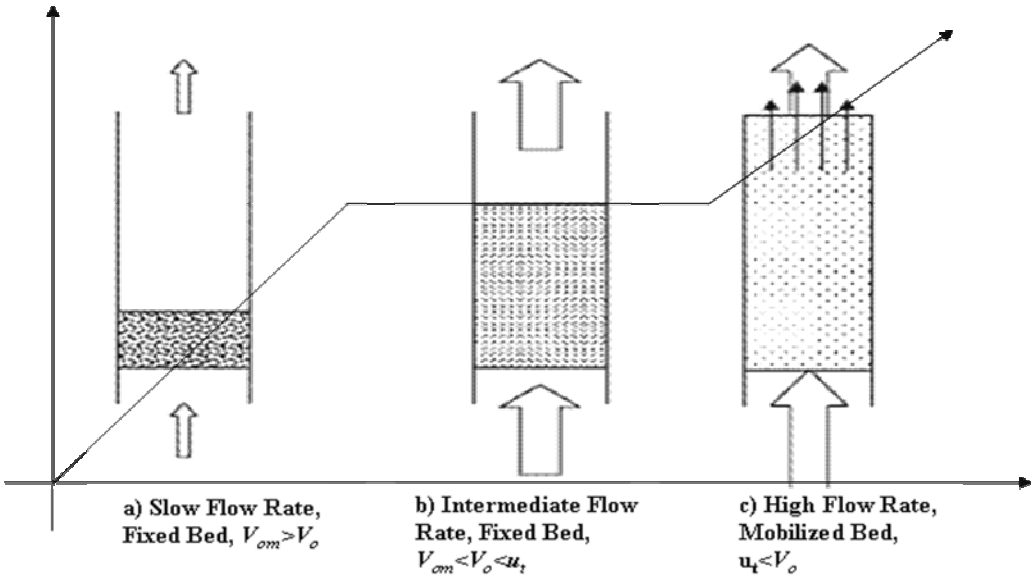

Figure 2.2 The phenomenon fluidization in fluid bed

2.1.3 Fluidization Regimes

When solid particles are fluidized, the fluidized bed behaves differently as velocity, gas and solid properties are varied [5, 16, 17]. It has become evident that there are number of regimes of fluidization, as shown in Figure 2.2. When the flow of a gas passing through a bed of particles is increased continually, a few vibrate, but still within the same height as the bed at rest. By increasing the gas velocity, a point is reached where the drag force imparted by the upward moving gas equals the weight of the particles, and the void of the bed increases

slightly. The velocity of the air this point, the onset of fluidization called minimum fluidization U_{mf}., Figure 2.2B. Increase gas flow further, and formation of fluidization bubbles sets. At this point, a bubbling fluidized bed occurs as shown in Figure 2.2C. As the velocity is increased further still, the bubbles in a bubbling fluidized bed will coalesce and grow as they rise. If the ratio of the height to the diameter of the bed is high enough, the size of bubbles may become almost the same as diameter of the bed. This is called slugging Figure 2.2D. If the particles are fluidized at a high enough gas flow rate, the velocity exceeds the terminal velocity of the particles.

The upper surface of the bed disappears and, instead of bubbles, one observes a turbulent motion of solid clusters and voids of gas of various sizes and shapes. Beds under these conditions are called turbulent beds as shown in Figure 2.2E. With further increases of gas velocity, eventually the fluidized bed becomes an entrained bed in which we have disperse, dilute or lean phase fluidized bed, which amounts to pneumatic transport of solids [42, 44].

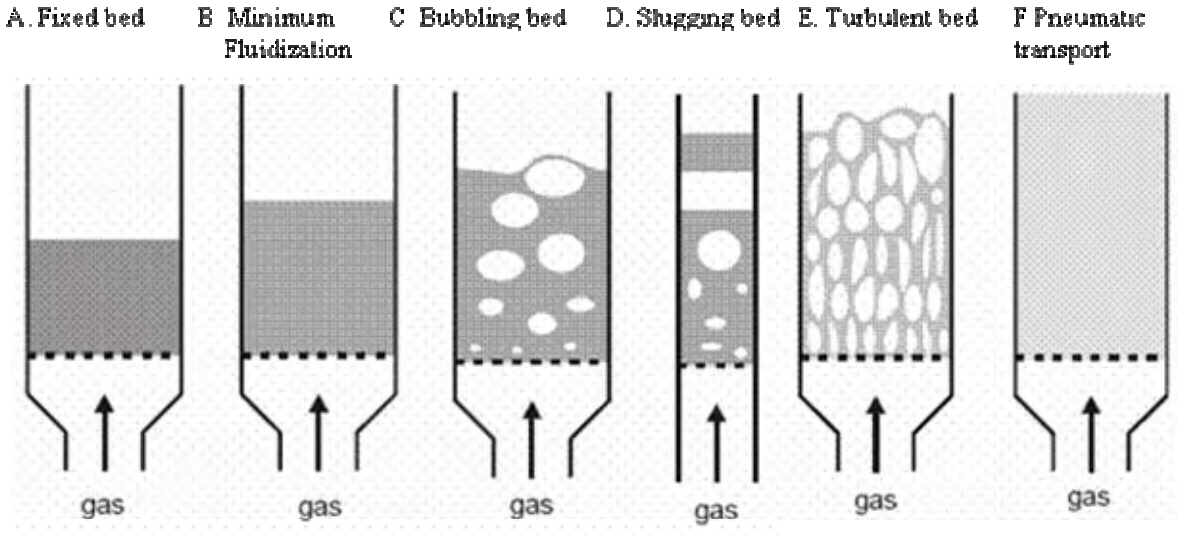

Figure 2.3 Schematic representations of fluidized beds in different regimes [5]

2.1.4 Minimum Fluidization Velocity

The transition between the fixed and fluidized bed states is rather gradual and somewhat ill-defined. Consequently, several definitions can be found in the literature for the minimum fluidization velocity. Other defined the minimum fluidization velocity as the gas velocity at which bed expansion begins [5,17].

The value of U_{mf}. is sensitive to particle's shape, density, and size. There are three basic approaches to obtain equations to calculate the minimum fluidization velocity.

An equation for the minimum fluidization velocity can be obtained from the Ergun equation (Pressure Drop) [5, 16].

For fixed bed,

$$\frac{\Delta P}{L} = 150\frac{\left(1-\varepsilon_{mf}\right)^2}{\varepsilon_{mf}^3}\frac{\mu U_{mf}}{\left(\phi_s d_p\right)^2} + 1.75\frac{\left(1-\varepsilon_{mf}\right)}{\varepsilon_{mf}^3}\frac{\rho_g U_{mf}^2}{\phi_s d_p} \tag{2.1}$$

and for fluidized bed,

$$\frac{\Delta P}{L} = \left(1-\varepsilon_{mf}\right)\left(\rho_p - \rho_g\right) g \tag{2.2}$$

where ΔP is pressure drop cross the fluid bed; L length of cylindrical particle; U_{mf} minimum velocity; ϕ_s, sphericity factor, μ viscosity; ε_{mf} void fraction; d_p particle diameter; ρ_g gas density, ρ_p particle density.

Combining equations 2.1, and 2.2 it is obtained a quadratic equation that describes the minimum fluidization velocity.

$$150\frac{\mu U_{mf}\left(1-\varepsilon_{mf}\right)}{\left(\phi_s d_p\right)^2 \varepsilon_{mf}^3}+1.75\frac{\rho_g U_{mf}^2\left(1-\varepsilon_{mf}\right)}{\phi_s d_p \varepsilon_{mf}^3}=g\left(\rho_p-\rho_g\right) \tag{2.3}$$

For the minimum fluidization velocity of very small particle, only the laminar flow term of the Ergun equation is significant. With Reynolds less than one, the equation for minimum fluidization velocity becomes

$$\frac{1.75}{\varepsilon_{mf}^3 \phi_s}\mathrm{Re}_{p,mf}^2+\frac{150\left(1-\varepsilon_{mf}\right)}{\varepsilon_{mf}^3 \phi_s^2}\mathrm{Re}_{p,mf}=\mathrm{Ar} \tag{2.4}$$

where the Archimedes number is defined as

$$\mathrm{Ar}=\frac{d_p^3 \rho_g\left(\rho_s-\rho_g\right)g}{\mu^2} \tag{2.5}$$

and

$$\mathrm{Re}=\frac{d_p U_{mf}\rho_g}{\mu} \tag{2.6}$$

In the special case of very small particles, equation 2.3 simplifies to

$$U_{mf}=\frac{d_p^2\left(\rho_s-\rho_g\right)g}{150\mu}\frac{\varepsilon_{mf}^3\phi_s^2}{1-\varepsilon_{mf}}, \quad \mathrm{Re}_{p,mf}<10 \tag{2.7}$$

For very large particles,

$$U_{mf}^2=\frac{d_p\left(\rho_s-\rho_g\right)g}{1.75\rho_g}\varepsilon_{mf}^3\phi_s, \quad \mathrm{Re}_{p,mf}>1000 \tag{2.8}$$

When ε_{mf} and/or ϕ_s are not know, one call estimate U_{mf} for a bed of irregular particle with no seemingly longer or shorter dimension as follows. First, rewrite equation 2.4 as

$$K_1\mathrm{Re}_{mf}^2+K_2\mathrm{Re}_{mf}=\mathrm{Ar} \tag{2.9}$$

where,

$$K_1 = \frac{1.75}{\varepsilon_{mf}^3 \phi_s} \quad \text{and} \quad K_2 = \frac{150\left(1-\varepsilon_{mf}\right)}{\varepsilon_{mf}^3 \phi_s^2} \tag{2.10}$$

When applying the Ergun equation, one has to know the minimum fluidization void, ε_{mf}, although it is frequently unknown. Wen and Yu [20] developed an expression for the minimum fluidization velocity for a range of particle types and sizes by assuming the following approximations shown in Table 2.1 to hold based on experimental [5]. They combined these with the Ergun equation and obtained the relation:

$$\mathrm{Re}_{mf} = \frac{d_p . U_{mf} . \rho_g}{\mu} = \sqrt{33.7^2 + \frac{0.0408 d_p^3 . \rho_g . \left(\rho_s - \rho_g\right) . g}{\mu^2}} - 33.7 \tag{2.11}$$

Another widely used expression obtained empirically another for fine particle is:

$$U_{mf} \approx 7.90 x 10^{-3} d_p^{1.82} \left(\rho_s - \rho_f\right) 0.94 \mu_f^{-0.83} \tag{2.12}$$

This equation is valid for $\mathrm{Re}_{mf} \leq 10$, whereas for higher values of Re_{mf} a correction factor must be applied.

In the special case of very small particle the minimum velocity can be obtained from:

$$U_{mf} \approx \frac{d_p^2 \left(\rho_s - \rho_g\right) g}{150 \mu} \frac{\varepsilon_{mf}^3 \phi_s^2}{1-\varepsilon_{mf}} \tag{2.13}$$

where, d_p particle diameter, ρ_g gas density, ρ_s solid density, μ gas viscosity, and g gravity.

Table 2.1 Values of the two constants for equation 2.9

Reference	First ($K_2/2K_1$)	Second ($1/K_1$)
Wen and Yu [20]	33.7	0.0408
Richardson [10]	25.7	0.0365
Saxena and Vogel [11]	25.3	0.0571
Babu [12]	25.3	0.0651
Grace [13]	27.2	0.0408
Chistester et al. [14]	28.7	0.0494

2.1.5 Terminal Velocity

At high velocity, the aerodynamic haulage in the particles can be sufficiently large to transport it outside of the system. This phenomenon is called elutriation and the value can be computed from

$$U_t = \sqrt{\frac{4gd\left(\rho_s - \rho_g\right)}{3C_D\rho_g}} \tag{2.14}$$

Where the drag coefficient expression is:

$$C_D = \frac{4}{3}\frac{\left(\rho_p - \rho_g\right)}{\rho_g U_t} d\, g \tag{2.15}$$

where U_t terminal velocity, g gravity, d average diameter, ρ_s particle density, ρ_g gas density, and C_D drag coefficient, and where C_D is an experimentally determined drag coefficient. In general, Haider and Levenspiel find [5].

$$C_D = \frac{24}{\mathrm{Re}} + \left[1 + \left(8.171\mathrm{e}^{-4.0655\phi_s}\right)\mathrm{Re}^{0.0964+0.5565\phi_s}\right] \tag{2.16}$$

$$d_p^* = d_p\left[\frac{\rho_g\left(\rho_s - \rho_g\right)g}{\mu^2}\right]^{\frac{1}{3}} \tag{2.17}$$

The terminal velocity

$$U_t^* = U_t\left[\frac{\rho_g^2}{\mu\left(\rho_s - \rho_g\right)}\right]^{\frac{1}{3}} \tag{2.18}$$

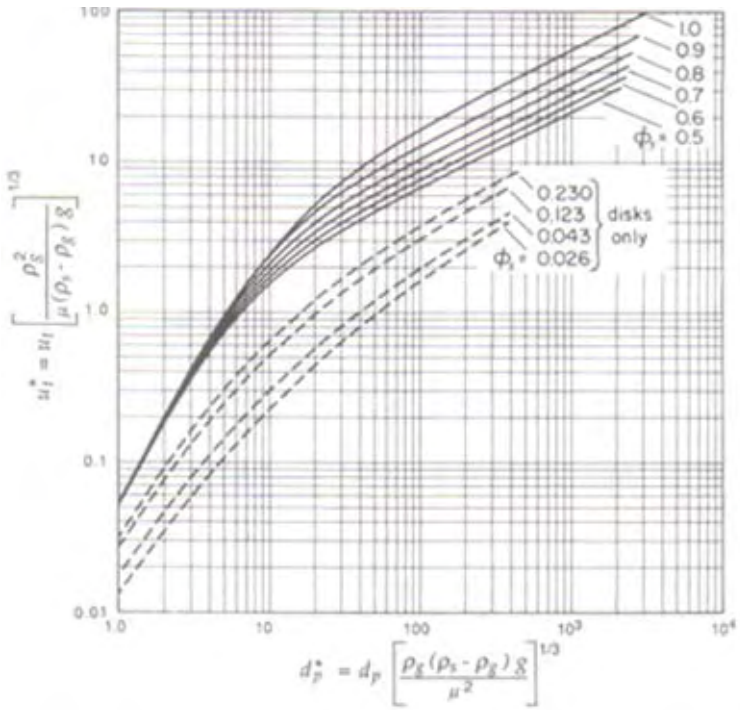

Figure 2.4 Chart for determining the terminal velocity of particles [5]

2.1.6 Minimum Bubbling Velocity

The superficial gas velocity at which bubbles first appear is known as the minimum bubbling velocity [46].

$$U_{mb} = K_{mb} d_s \tag{2.19}$$

and

$$U_{mb} = \frac{2.07 e^{0.716F} d \rho_s^{0.06}}{\mu^{0.347}} \tag{2.20}$$

where U_{mb} minimum bubbling velocity, K_{mb} constant, d_s solid diameter, F fine fraction, μ dynamic viscosity, ρ_s solid density.

2.2 Fluid Bed Dryers

Small batch fluid-bed dryers are commonly used for drying pharmaceutical powders. According to the type of the material, appropriate fluidized-bed systems are chosen. Due to better air-solid contact, drying in fluid bed dryers is faster than in tray ovens and because of good mixing, product uniformity is much improved [19, 38]. A fluidized bed is essentially non-homogeneous [6, 19, 38]

A bed may be well fluidized if all the particles are fully supported by the gas, but may still be segregated in the sense that particles with lower density will migrate to the surface whereas those with higher density will migrate to the distributor base. Many models have

been proposed to predict the axial distribution of particles with different sizes in a fluidized-bed [5, 19, 38].

The FBD where solids are fluidized by the drying gas find applications in a variety of drying problems [19, 38].

2.2.1 Fluidization Pattern in the Fluidized Bed Dryer

The fluidized bed has a non linear aerodynamic behavior with a bubbly movement. The movement of the particles corresponds to the movement of the phases of the fluid that has been modeled for particles [16, 17]. An extended variety of experiments have been reported to study the influence that interior forces have on the fluidized beds [19].

Fluidizations patterns have been analyzed using the gas theory of chaos, using dominant frequencies to analyze by FTIR spectroscopy [19]. Fluidization is for purposes of the active ingredient for respective fluidized particle along with the control of the particles [21]. The evaluation of the movement and distribution of the particles in the fluidization is a fundamental aspect. This action impacts on the culmination of the elaboration of the products and the quality of the product that is obtained. The complementary evaluation of the dynamic fluid shows maximum pressure, low amount in both components of the particles the micronized lactose and naproxen sodium crystallized [22].

The weight has to be evaluated in fractions and sizes of powders of through group C in the fluidized bed [23]. Movement has to do with the nonlinear interactions of two

independent media with own movements and tendencies, also pertinent in the individual movement of the fluids and particles [24, 25, 26].

There is a lot of interest shown in the biochemical world due to recent advances. Many researchers are developing novel particles to manufacture medicines for asthma [27, 28, 29].

2.2.2 Drying Process

In the fundamental drying process, regardless the type of dryer and of the solid particle a four phase sequence occurs as shown in Figure 2.5. First, the drying air and the material are heated to the drying temperature, and then moisture from its surface is evaporated, after the particle is partially dry, it goes to the next phase. Finally, the particle surface is completely dried through a combination of internal evaporation and diffusion. It is very important to know the different phases of the materials dried in the fluid bed. The four different phases are shown in Figure 2.5.

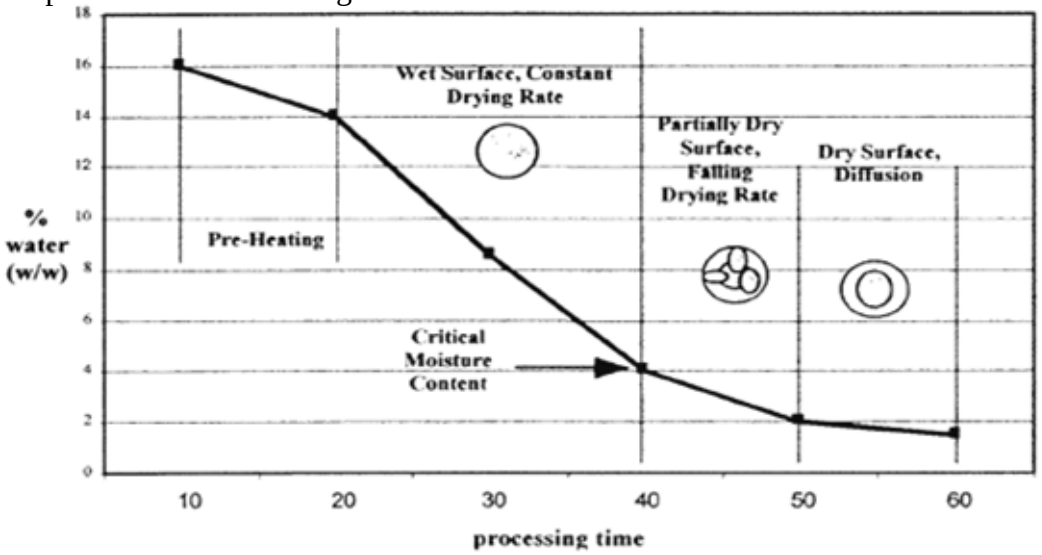

Figure 2.5 Typical moisture content in product (%w/w) vs. processing time curve [38]

When heat is added two effects occur at the same time. During the initial adjustment, the rates of heating and cooling become equal and then the temperature of the drying material stabilizes. After the material stabilizes, the diffusion phase of the curve is constant. The diffusion phase is characterized by a constant drying rate of moisture from the surface. This occurs because the solid is initially very wet the surface is completely covered with a liquid. The liquid is entirely unbound moisture.

The dying process is characterized by a transition from a constant drying rate to a falling drying rate period. This is identified by critical moisture; and the phenomenon is due, in part, by the surface of the particle. The long path is necessary for the water to migrate to surface of the particle. The average moisture content of the solid reaches the critical moisture content, the surface film of moisture is reduced by evaporation that further drying causes dry spots to appear upon the surface. These dry spots appeared because the surface water is no longer replaced at that rate. This is not fast enough to maintain a continuous film at the particles surface.

Fluidized beds exhibit a uniform temperature distribution due to the vigorous mixing provided by the random motion of the bubbles. Since the particle surface area is very fine, fluid-to-particle heat and mass transfer is rarely a limiting factor in the design and control of fluidized bed as the heat transfer between surfaces and the fluid – solids is. Therefore, the knowledge of these heat transfer rates is of fundamental importance in the design and control of fluidized bed, if the aim is to optimize the performance of the internals used for cooling and heating of the fluid-particle system.

Among many gas-solid flow systems involving heat and mass transfer operations, the fluidization system is one of the most frequently encountered. The heat and mass transfer behavior in a gas –solid fluidized bed is important when physical or chemical operations are conducted in the bed, such as drying, coal combustion, polymerization reaction, and chemical synthesis. The inherent intensive gas - solid contact or rapid mixing between gas and solid phases contributes to this efficient heat transfer. The fluidized bed possesses high heat capacity, and uniform temperature in the bed can generally be maintained. Thus, temperature control in the bed can be effectively carried out. Comparable characteristics are also exhibited for the fluidized bed mass transfer between gas and particles in the FBDU [37].

2.2.3 Single Particle Model of Heat and Mass Transfer

The single particle model postulates that the moving solid particles play an important role in heat transfer by thermal conduction. The model takes into account the thermal conduction through the layer of gas at the heating surface.

The simplest model of this kind can be represented by Fourier equation of thermal conduction can be expressed as [5, 17].

$$\rho_p c \frac{\partial T_p}{\partial t} = K_p \nabla^2 T_p \tag{2.21}$$

For the particle phase

$$\rho c_p \frac{\partial T}{\partial t} = K \nabla^2 T \tag{2.22}$$

For the gas phase

The boundary and initial condition for equation (2.19) and (2.20) are given by the following:

At the symmetric plane

$$\frac{\partial T_p}{\partial n} = 0 \quad ; \quad \frac{\partial T}{\partial n} = 0 \tag{2.23}$$

At the heating surface

$$T_p = T_s \quad ; \quad T = T_s \tag{2.24}$$

At the gas particle interface

$$K_p \frac{\partial T_p}{\partial n'} = K \frac{\partial T}{\partial n'} \tag{2.25}$$

Far inside the bed

$$T = T_b \tag{2.26}$$

At t = 0 (initial condition)

$$T = T_p = T_b \tag{2.27}$$

Where K_p thermal conductivity of particles, K thermal conductivity of gas, T_p temperature of particle, T_s temperature of the heating surface, T_b bed temperature ρ_p density particle, c_p specific heat at constant pressure, c specific heat of particles, n coordinate normal to the temperature symmetric plane , n' coordinate normal to the gas particle interface, and ∇^2 gradient [17].

The gas particle mass transfer, under fairly low gas velocity conditions where V is close to U_{mf} or the bed is in particle fluidization, the plug flow assumption for the gas phase can be reasonably made. The mass balance on the concentration for species A in the gas phase, C_A, over the incremental height dh can be expressed as [17]

$$V\frac{dC_A}{dh} = k_f S_B \left(C_A^S - C_A\right) \tag{2.28}$$

Where C_A^S is the saturation concentration of species A on the solid surface and k_f is the particle to gas mass transfer coefficient, S_B surface area of solid per unit volume of the bed.

2.3 Crystallization

The crystallization process factors important for particle reduction by crystallization are: naproxen sodium solution, fluidization temperature, crystallization time, aspersion pressure, and fluidization velocity [16, 30].

Crystallization is a process that produces solids from a supersaturated solution. Supersaturation occurs when the concentration of dissolved solute in a solution exceeds its thermodynamic equilibrium concentration. This condition is normally expressed in terms of differential temperature, concentration or concentration rate depending on the concentration, temperature and rates of addition and mixing, the addition and salting out of anti-solvent can result in crystallization or precipitation.

Depending on the concentration, temperatures and rates of addition and mixing, the addition and salting out of anti-solvent can result in crystallization or precipitation.

Pharmaceutical solids may come in contact with water during processing steps, such as crystallization by fluid bed dryer at high vacuum pressure. Evaporated water molecules and ethanol molecules may reside on crystal surfaces or in crystal lattice structures, but when the absorbed water enters the lattice structure it can change the packing in the unit cell, resulting in the formation of crystallized naproxen sodium.

Crystallization refers to the formation of solid crystals from a homogeneous solution. It is essentially a solid-liquid separation technique and a very important one at that [16, 30, 40]. Crystals are grown in many shapes, which are dependent upon downstream processing or final product requirements. Crystal shapes can include cubic, tetragonal, orthorhombic, hexagonal, monoclinic, triclinic, and trigonal. In order for crystallization to take place a solution must be supersaturated. Supersaturation refers to a state in which the solvent contains more dissolved solute than can ordinarily be adequate at that temperature [15, 29]. The crystallization is normally carried out either from a solution or from a melt, occasionally crystals are formed directly by condensation from a vapor to a liquid which is also common to crystallization [16, 30].

The crystallization process consists essentially of two stages which generally proceed simultaneously but which can to some extent be independently controlled. The first stage is the formation of small particles or nuclei, and the second stage is the growth of nuclei. If the nuclei number can be controlled, the size of the crystals ultimately formed can be regulated, and this forms one of the most important features of the crystallization process [16, 30].

Figure 2.6 depicts the crystallization as a function concentration versus temperature.

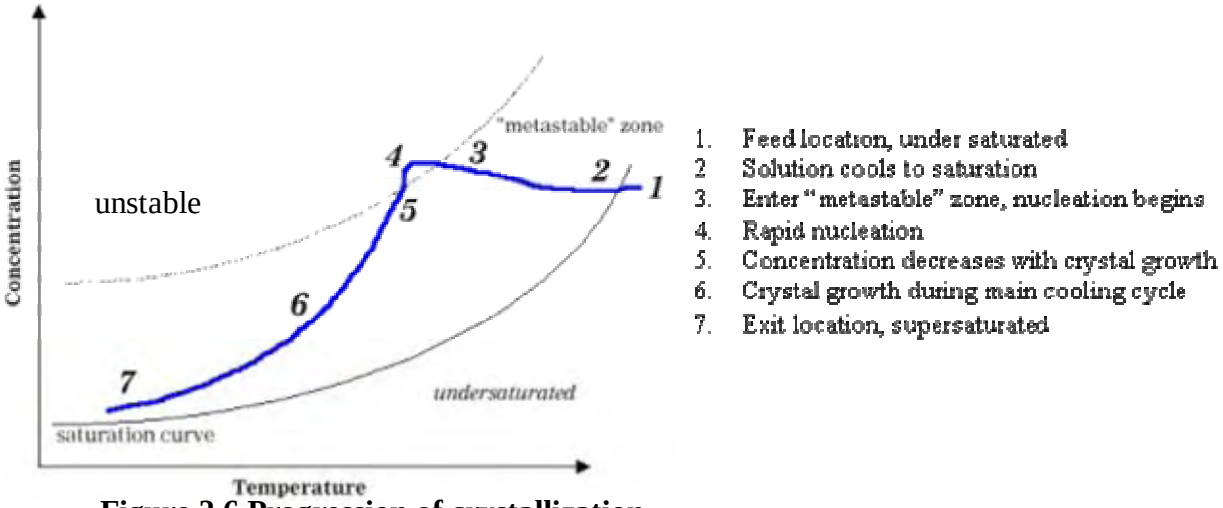

Figure 2.6 Progression of crystallization

Types of crystallization are: by cooling, by evaporation, by reaction, by salting-out, and by vacuum.

The diagram stays divided in three zones:

1. Stable zone (sub-saturated), where no crystallization is possible.
2. Metastable (supersaturated), between the curves of supersaturation and solubility, where the crystallization occurs by growth of crystals that are already present in the dissolution.
3. Unstable zone (supersaturated), where the crystallization is spontaneous.
    - When $S<1$, ΔG is always positive, not new phase is not formed spontaneously.
    - For $S>1$, ΔG has a maximum positive at a certain critical radius. The height of this maximum is the necessary energy for the nucleation activation.

- The older embryos which their size is critical will diminish their free energy due to the growth, and then they give room to stable nucleus that grows to form microscopic particles.

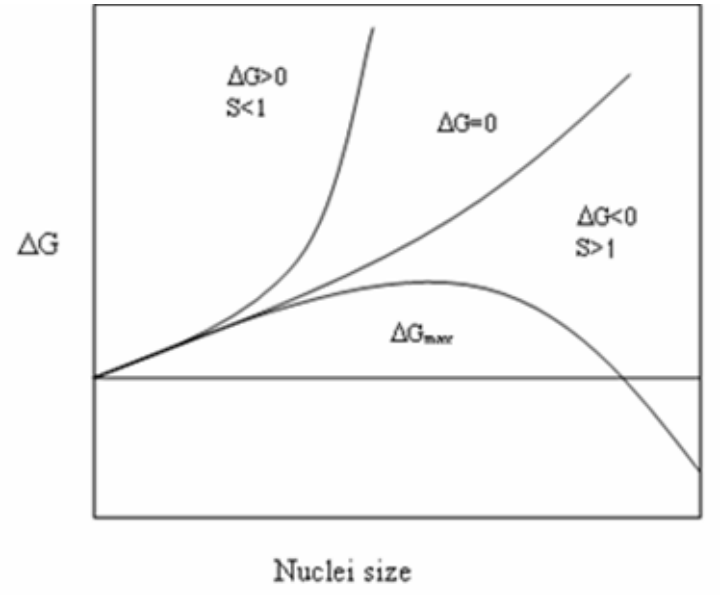

Figure 2.7 Growth crystallization

2.3.1 Nucleation Kinetic

Primary nucleation often occurs in solutions with high levels of supersaturation, resulting in large number of small particles that compete for growth. If an explosion of fine particles occurs during the initial crystallization event from an unseeded batch system, it may be difficult to grow an acceptable size distribution. The high surface area of the fines complicates the growth process as additional solute becomes crystallized.

The driving force for crystallizations in most industries is by secondary contact nucleation, whereby the nuclei result from crystal to crystal. This phenomenon occurs at relatively low levels of supersaturation, and affords better control of the nucleation.

Secondary nucleation is influenced by the level of supersaturation, hydrodynamics, power input, shear forces, type of agitator and solids concentration.

Empirical kinetic equation for the competing phenomena of growth and nucleation are as follows:

$$G = \frac{dL}{dt} = k_g S^g \tag{2.29}$$

where G is growth and nucleation, L is a characteristic dimension, t is time, k_g is a function of fluidization, temperature, solution; S is supersaturation; and g is the exponent for the growth is dependence on solution.

2.3.2 Growth Rate

The growth rate of a crystal in a solution is depends on the temperature and concentration of the liquid at the crystal face. These conditions are not generally the same as those in the bulk of the solution. However, gradient concentration is necessary for the transfer of solute toward the face, and temperature gradient for the dissipation of the heat of crystallization [48].

The rate of crystallization is a function of the degree of super-saturation. For crystallization from a melt, process depends on the rate of transfer of heat between the crystal face. The equation for crystallization is:

$$B^0_{\text{hom}og} = \left.\frac{dN}{dt}\right|_{nucli} = A\exp\left(-\frac{\Delta G}{RT}\right) \tag{2.30}$$

and

$$B^0 = A\exp\left[-\frac{16\pi\sigma^3 V_m^2}{3k^3T^3\left(\ln S\right)^2}\right] \tag{2.31}$$

where B^0 rate crystallization, N number nuclei, ΔG Gibbs energy change, A factor (10^{25}) k Boltzmann constant, T temperature, V_m molar volume, S supersaturation, σ superficial energy (solid – liquid).

Crystallization involves several competing mechanisms. Newly generated solids can be employed to produce nuclei or to grow existing crystals. Nucleation results in the generation of submicron size particles or nuclei. The primary mechanisms, those in which the product crystals do not participate, can be either homogenous or heterogeneous.

The important factors in crystallization are solution concentration, temperature, solids concentration, external equipment, crystallization kinetics, solution pH, hydrodynamics, agitation, Feed inlet location, residence time.

2.4 Particles Adhesion

Particle adhesion is the result of forces which exist between particles and a solid surface in contact, where the solid surface can be a particle surface itself [32, 33]. Dry adhesion can be observed for surfaces in contact under vacuum or any other environment that completely excludes adsorption or capillarity condensation in the contact zone. Boundary

adhesion occurs, if the gap between the surfaces in contact is so narrow that the properties of the contact spot differ from the properties of the separated surfaces. Static adhesion is measured applying a minimum force required for detachment at an infinitely slow rate, while dynamic adhesion is determined applying a detachment force at a finite rate. In the latter case the force measured is detachment rate dependent and also changes with increasing distance between the contiguous surfaces [34, 35, 45].

The adhesion refers to the fundamental atomic and molecular forces that are responsible for keeping two phases together. The term contact mechanics, on the other hand, is used to describe the behavior of solids in contact when subject to an external load. The applied loads, the internal adhesive forces, the material properties and the system geometry all influence the contact behavior of solid materials. The study of adhesion requires the characterization of surfaces and interfaces, as adhesion emanates from the surface forces acting between various surfaces. A number of different surface analytical techniques have been developed to characterize surface forces, and to study the adhesion phenomena is very important [26, 36].

The solid bridges are formed by crystallization of liquid bridges which contain solvents; solidification of swelled ultra fine particles; freezing of liquid bridge bonds, chemical reactions with adsorbed surface layers with interstitial pore water; solidification of high viscous bond agents; contact fusion by sintering chemical bonds by solid–solid reactions. Interlocking by macromolecular and particle shape effects: interlocking of chain branches at macromolecules; interlocking of contacts by overlaps of surface asperities; interlocking by hook-like bonds. Figure 2.8 shows the adhesion particles.

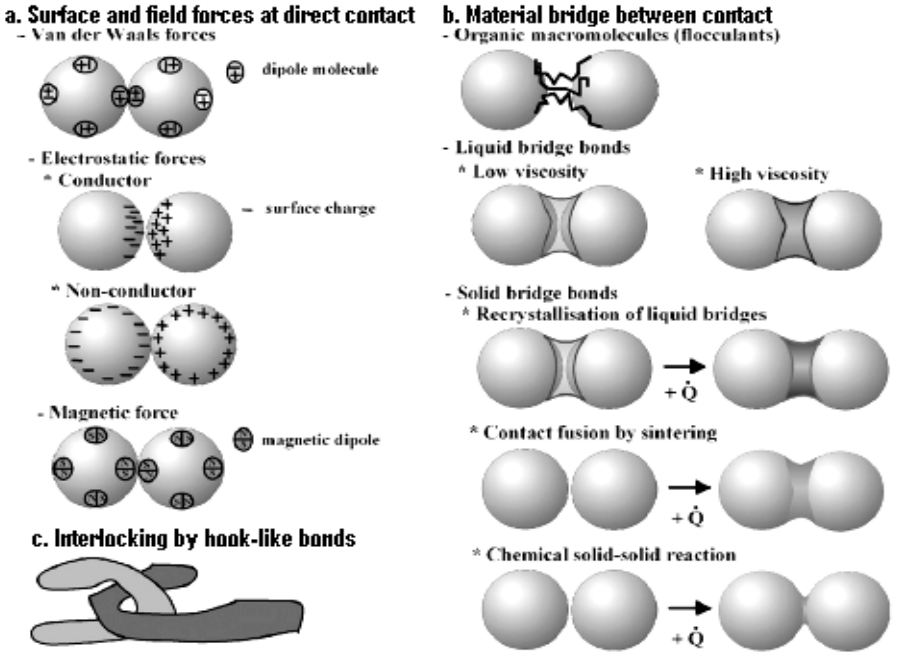

Figure 2.8 Particle adhesion and micro processes of particle bond effects in contact [26]

The particles that have positive charge are attracted by Van der Waals forces forming dipoles, because the charges are positive in the surface [35, 47].

The particles that have positive and negative charges are attracted by electrostatic forces. This occurs because the charges are superficial to the particle. The particles that have negative charges are distributed in all the surfaces then are attracted with difficulty. Due to the weak forces between the particles, magnetic fields are formed. The particles can be adhered by interlock because of their shape and morphological structure [35, 47].

The contact forces shown in the Figure 2.9 helped on the analysis to the identification of the forces being in contact between particles CNS and the MCL functionalized process.

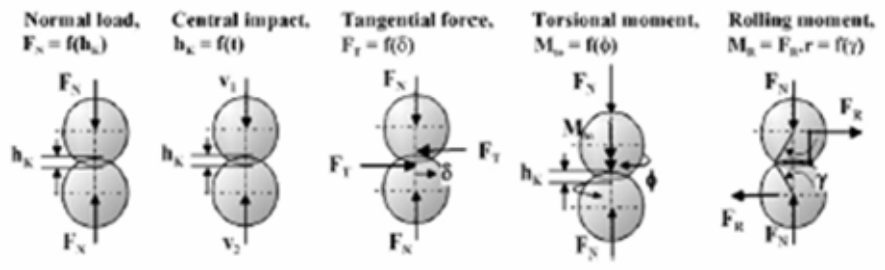

Figure 2.9 Particle contact forces [26].

2.4.1 Forces causing Adhesion of particle to particles of surfaces

a. *Lifshitz –van der Waals forces*, the long-range interaction between molecules, collectively known as the van der Waals force consists of 3 main types of forces, which are the Dedye - induction force, the Keesom - orientation force. The induction and orientation forces are the characteristic forces for dipole molecules [35, 36].

b. *Capillary forces* are of great importance for powder flow. Moist powders usually exhibit poor flow properties, and they tend to stick to the metal walls of chamber or any other surface in contact during powder handling [35, 36].

c. *Electrical forces* are the consequence of the contact between particles or a particle and a surface. They are related to the difference in contact potential, and in dry enviroent are associated only with particles below 5 μm [35, 36].

d. *Electrostatic image forces*. Generate electric dipole [35, 36].

2.4.2 Factors Influencing Adhesion

a. *Surface Roughness.* One of the important mechanisms affecting the adhesion forces between particles and surfaces is the geometry of the contact between them. The geometry of contact is strongly related to the roughness of the surfaces in contact. Real contact occurs only at the crest of the surface asperities, where the local contact pressure is very high [34].

b. *Work of Adhesion and Surface Free Energy.* One major factor to consider in solid-solid contact is the work of adhesion. Physically, the work of the adhesion is defined as the free energy change required to separate unit areas of two surfaces from contact to infinity in vacuum. For surfaces of different materials the energy is called "work adhesion" whereas for surfaces of identical materials the correct terminology is work adhesion [34].

c. *Hardness and Elasticity* of materials and the influence of plastic, elastic and viscoelastic, deformation of the materials on adhesion [34].

d. *Particle size and shape.* The influence of particle size on the adhesion force cannot be described in simple general terms, as it depends on, for example, the surface roughness of the substrate surface, particle shape and physical type of force involved in the adhesion process [34].

2.5 Application of Functionalized Particle

The inhalation treatment is administered fundamentally, using inhalers by metered doses that are pressurized. Metered doses constitute approximately eighty percent of the inhalers, and the other twenty percent of the inhalers contain dry powder [2, 3, 37]. Physicians prefer to prescribe inhalers for lungs diseases. The advantages inhalers of inhalers is that they act naturally as a filter, making it easy for the particles to go into the deep air flow passages of the lungs, and unblock them. The results are high concentrations of particles in the air pathways [2, 3].

The inhalation treatment is administered fundamentally, using inhalers by metered doses that are pressurized. Metered dose inhalers constitute approximately eighty percent of the inhalers, and twenty percent of the inhalers that contain dry powder. Selecting the appropriate treatment for lungs diseases, physicians prefer to prescribe inhalers. The advantages inhalers have are that they act naturally as a filter. Thus, making it easy for the particles to go into the deep air flow passages of the lungs, and unblock them. The results are high concentrations in the air pathways [2].

3 MATERIALS AND METHODOLOGY

3.1 Equipment

3.1.1 Fluidized Bed Dryer (FBD)

The airflow enters from the bottom part of the fluid bed dryer. In the superior part of the equipment there are four filters to avoid the loss of the fine particles. The fluid bed processing unit can be operated manually and automatically during fluidization process. Figure 3.1 shows specific details of the fluid bed process. See Appendix A.

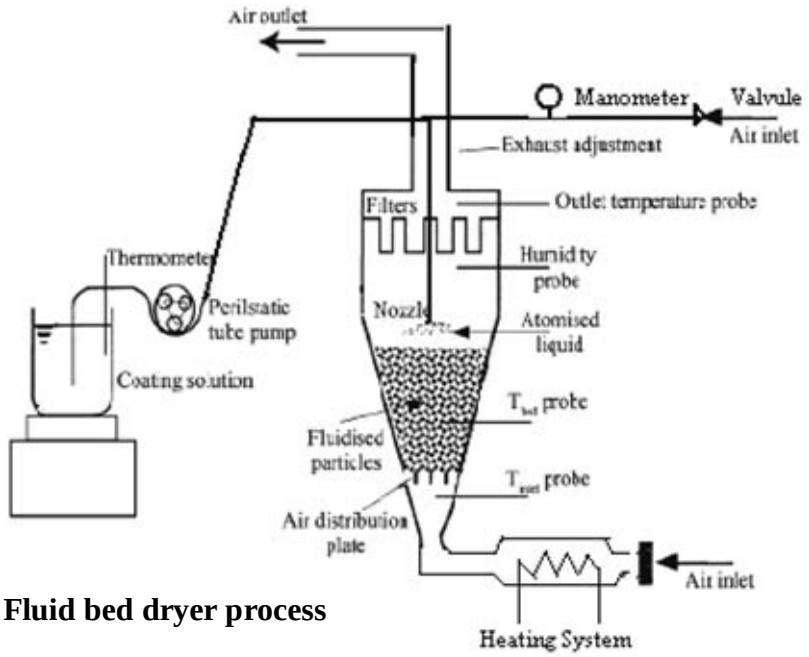

Figure 3.1 Fluid bed dryer process

A variable speeds pump drive; is utilized to feed the solution into the chamber. The temperature control by means of a PID controller.

The chamber has a conical and cylindrical shape that helps support the fluidization process, the dimension show in Figure3.2. The sieve, model 2300 S/S 304, is located at the bottom of the chamber, and its purpose to provide an adequate air flow distribution.

Figure 3.2 depicts chamber of fluid bed processing unit dimension details.

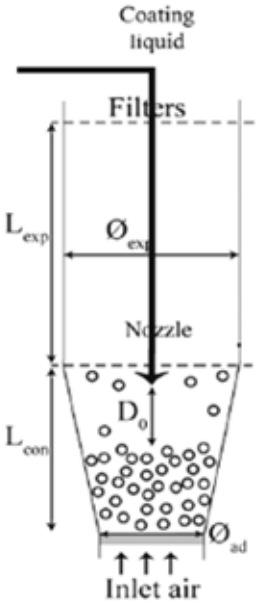

Dimension

- L_{exp}: 21.00 cm
- L_{con}: 19.40 cm
- ϕ_{exp}: 15.20 cm
- ϕ_{ad}: 8.10 cm

Figure 3.2 The chamber of fluid bed dryer process dimension

3.1.2 Nozzle

The nozzle used is a model PJ8 of 303 stainless steel, typical pressure range of 260.67 kPa to 6892.86 kPa, typical flow rate range is 6.3×10^{-4} at 0.0882 L/s, drop size is finest, spray angle 90º and spray pattern fog. Figure 3.3 illustrates the nozzle characteristic.

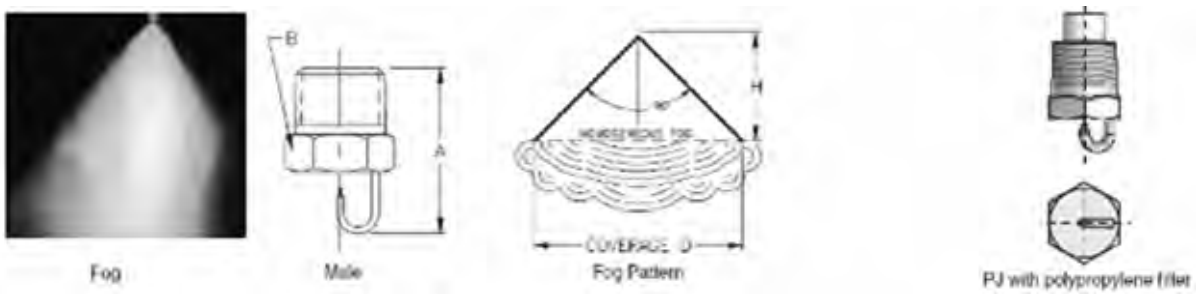

Figure 3.3 Nozzle PJ8 make of BETE

3.1.3 Pump

The pump used were Model 75211-10, 50-5000 RPM. Frequency 50 to 60 Hz, powder 1.0 HP and intensity of 2.0 amperes and pressure to 2067.85 kPa.

3.1.4 Operating Parameters used in the Fluid Bed Processing Unit

The minimum fluidization airflow was 0.2 m/s and maximum fluidization of airflow was 5 m/s in the fluid bed process. The operation parameters are shown in the following Table 3.1:

Table 3.1 Adequate operating parameter in FBPU

Parameter	Setting
Peristaltic Pump	60 RPM
Nozzle diameter PJ8	2.032×10^{-4} (0.008 in)
Wurster insert	Spray
Atomization air pressure	551.43 kPa (80 psig)
Temperature solution	313.15 K(40°C)
Preheating temperature	313.15 K (40°C)
Aspersion time	30 s
Dry time	600 s (10 min)
Batch size (MCL)	0.001 kg (10 g)
Spray rate	1.0 mL/s
Inlet temperature	313.15 – 318.15 K (40-45 °C)
Bed temperature	311.15 – 315.25 K (38-42 °C)

Table 3.2 Materials properties

Material Properties			
Details	**Symbols**	**Value**	**Units**
• Gas density	ρ_g	1.2×10^{-3}	g/cm^3
• Particle density	ρ_s	1.53	g/cm^3
• viscosity	μ	1.8×10^{-4}	g/cm.s
Particle diameter average			
• Particle diameter(MCL)	d_L	2.349	μm
• Particle diameter(CNS)	d_C	2.28	μm
• Particle diameter(FP)	d_F	4.04	μm
• Sphericity	ϕ_s	1.00	
• Void fraction	ε	0.55	

3.2 Instruments

3.2.1 Scan Electron Microscope (SEM)

The Scanning Electron Microscope (SEM) model Joel SEM 6390, has a secondary detection electron device. It has a range of 100 nm to 2 mm, and was set to 10 kV, 10-30 SEI. The SEM was used to determine the particle sizes, morphology of MCL, NS, CNS, and functionalized particle.

3.2.2 Energy Dispersive X-Ray Microanalysis (EDAX)

The Energy Dispersive X-Ray Microanalysis (EDAX) model XM4 Genesis, using DT 30% spot size diameter. It determines the active ingredient composition, based on the distribution scrutiny scale of functionalized particles.

3.2.3 Fourier Transform Infrared (FTIR)

The Varian 800 Fourier Transform Infrared (FTIR) spectrometer, was used for the analysis of experimental samples. This equipment determines the changes on the NS, CNS, particles functionalized (PF) in functional groups such as carbon - hydrogen, carbon – oxygen, carboxyl – hydrogen, carbon-carbon.

3.2.4 X-Ray Diffraction (XRD)

Crystals were analyzed and identified by X-Ray Diffraction (XRD) analysis using model Siemens D5000 Electric Parameters automatic powder diffractometer with APD 3720 analysis software. About 1 to 2 g of crystals was required. Each crystal sample was ground to a fine powder with a mortar and pestle before being pressed into the sample holder. Copper Kα radiation was used. The radiation for Copper Kα1 is 1.54056Å. The XRD patterns were made over a diffraction-angle (2θ) range of 4 - 80°, with a step size of 0.02 º and a counting time of 1 second per step.

3.3 Material Preparation

3.3.1 Lactose Monohydrate

Lactose monohydrate (MCL) is used in the pharmaceutical industry as an excipient for pharmaceutical products. The particle size has to be in the range 1.0 μm to 10 μm [3, 7]. The molecular weight is 360.32 g/mol and molecular formula $C_{12}H_{22}O_{11}.H_2O$. The physical characteristics are odorless white powder that is soluble in water, the specific gravity is 1.53, and the melting point is 214°C [49].

The density of the MCL was determined using tap density, obtaining a value of 1.53 g/cm^3.

3.3.2 Naproxen Sodium

Naproxen Sodium (NS) is an active ingredient which belongs to the non-steroidal anti-inflammatory drug family. Naproxen sodium reduces inflammation (swelling), pain, and temperature. Naproxen sodium is used to treat mild to moderate pain, osteoarthritis, rheumatoid arthritis, primary dysmenorrheal, tendonitis, bursitis, and other conditions [7].

The physical properties of Naproxen Sodium: (–)-Sodium (S)-6-Methoxy-alpha-methyl-2-naphthaleneacetate; molecular weigh: 252.24 g/mole; molecule formula: $C_{14}H_{13}O_3Na$; Na: 22.998 uma (weigh atomic); %Na: 9.11 percentage. Figure 3.5 shows its molecular structure. See Appendix B.

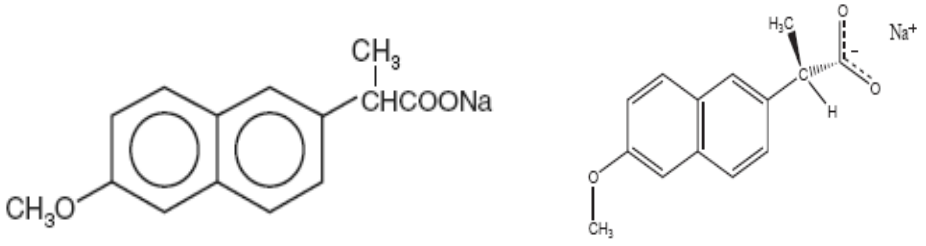

Figure 3.4 The structure formula of (S)-(+)- sodium naproxen

The typical average particle size of commercially available product is around 32 μm [49]. The measured solubility of sodium naproxen in pure water and in aqueous methanol solutions are listed in Tables 3.4 and 3.5 [40].

Table 3.3 Solubility of naproxen sodium in pure water [40]

Temperature (ºC)	Solubility (g sodium naproxen/kg solution)
9.10	78.90
16.90	128.60
23.10	186.50
27.20	240.20

Table 3.4 Solubility of naproxen sodium in water and alcohol [40]

Temperature (ºC)	Solubility (g sodium naproxen/kg solution)
27.90	240.20
28.30	246.10
30.30	273.70
34.10	308.10
36.90	333.70
39.70	364.10

3.4 Preparation for Aspersion Solution

The solution contained 30 mL (30% v/v) of ethanol (95% purity) and a density of 0.9243 g/mL, 70 mL (70% v/v) of water with a density 0.9884 g/mL, and 20g (20% w/w) naproxen sodium.

The solution was maintained at a temperature of 313.15 K (40°C) before entering the processing chambers.

3.5 Analysis of Variance (ANOVA)

Variables: Temperature (T_i), Pressure (P_i).

Fixed: Quantity of mass lactose, velocity fluidization, concentration active ingredient, time coating, and fluidization time.

The appropriate procedure for testing the equality several means is the analysis of variance. It is probably the most useful technique in the field of statistical inference.

The model for data, to describe the observation from an experiment with a model. One way to write this model is [38].

$$y_{ij} = \mu_i + \varepsilon_{ij} \tag{3.1}$$

An alternative way to write a model for the data is to define:

$$y_{ij} = \mu_{.} + \tau_{ij} + \varepsilon \tag{3.2}$$

Both the means model and the effect model are linear statistical models; that is, the response variable y_{ij} is the linear function of the model parameter. The data would appear as in Table 3.7

Table 3.5 Process data for a single factor experimental

Treatments	Absorbance of coating	
	Run 1	**Run2**
1	FP1	FP1
2	FP2	FP2
3	FP3	FP3
4	FP4	FP4

3.6 Experimental Procedure for Particle Functionalization

Figure 3.7 shows the different steps of the experimental procedure for particle functionalization.

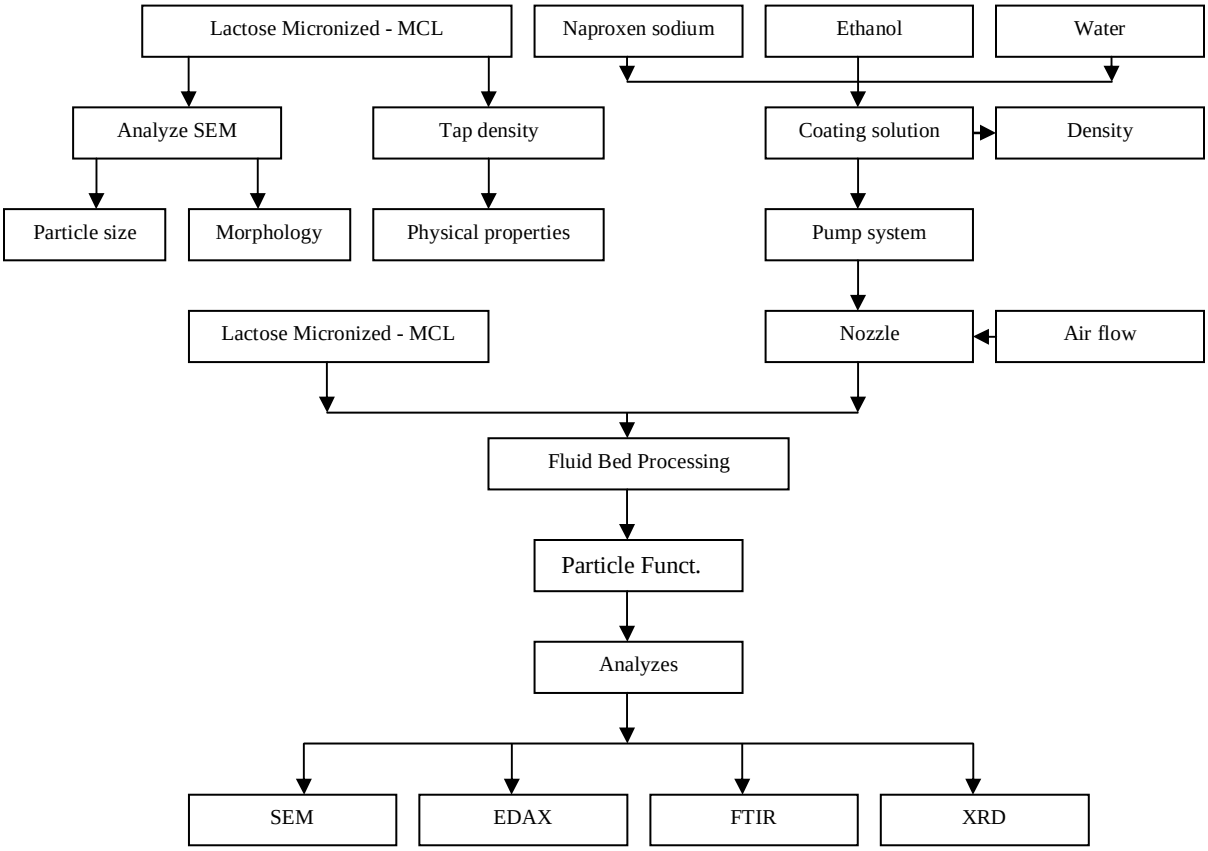

Figure 3.5 The experimental procedure for particle functionalization

1. Identify the physical, chemical properties of the micronized lactose, naproxen sodium using SEM, FTIR, and XRD.
2. Prepare the naproxen sodium solution at different concentration in water and ethanol maintaining constant a temperature.

3. Calibrate the fluid bed dryer.
4. Set and fix conditions to operate the equipment in the fluid bed dryer for optimal functionality in the fluid bed process.
5. Verify and set the control of the temperature, pressure, velocity of airflow, and set the aspersion fluid rate of nozzle in fluid bed dryer.
6. Monitor the aspersion of the nozzle, the airflow temperature, the active ingredient concentration in the solution, the solution temperature, fluidization velocity, fluidization time, functionalization time, and nozzle location in fluid bed dryer.
7. Feed the naproxen solution to the FBD for fluidization; the aspersion process is for 30 seconds.
8. Dry the precipitated particles for 10 minutes with the aspersion pump turned off.
9. Analyze the particle functionalized using SEM for determine morphology, composition with EDAX, particle size with FTIR, and the crystalline structure with XRD.

4 RESULTS AND DISCUSSION

4.1 Experimental Description

The experimental procedure followed included the reduction of the particle size of the NS by crystallization, determination of the corresponding operating conditions, and then the precipitation of CNS over MCL. The initial conditions of each of the raw materials were determined to compare later on with the treated material.

4.1.1 Velocities Calculation

The minimum velocity was computed using equation 2.13, the terminal velocity equation 2.18, the bubbling velocity equation 2.20, and operational velocity. The results are shown on the Table 4.1.

Table 4.1 System velocities

Velocities		Experimental valor	Theory valor	Relative error (%)	Units
Minimum velocity	U_{mf}	4.73	3.31	30.02	cm/s
Bubbling velocity	U_{mb}	1.18	0.66	44.00	cm/s
Terminal velocity	U_t	118.3	114.42	3.30	cm/s
Operational velocity	U	26.45	33.06	-25.00	cm/s

4.1.2 Dimensionless Numbers Calculation

The dimensionless numbers: Reynolds (Re) and Archimedes (Ar) were calculated from experimental data using the equations 2.5, and 2.6. The results are shown on the Table 4.2.

The Re Number confirmed that the flow is laminar, and the Ar Number established the buoyancy of the particles.

Table 4.2 Dimensionless numbers

Dimensionless Number	Results	
Reynolds number	$Re_{P,\ mf}$	$7.4\times10^{-3} < 10$
Archimedes number	$Ar_{P,}$	7.1×10^{-4}

4.2 Micronized Lactose (MCL)

4.2.1 Particle Size Distribution of Micronized Lactose

The MCL was donated by DMV-Fonterra Excipients (www.dmv-fonterra-excipients.com), through the Mutchler Ingredients Company.

Figure 4.1 depicts the particle size distribution (PSD) of MCL; the average particle size obtained was 2.349 µm, and standard deviation 0.9569 using Scan Electron Microscope (SEM) and Scandium software.

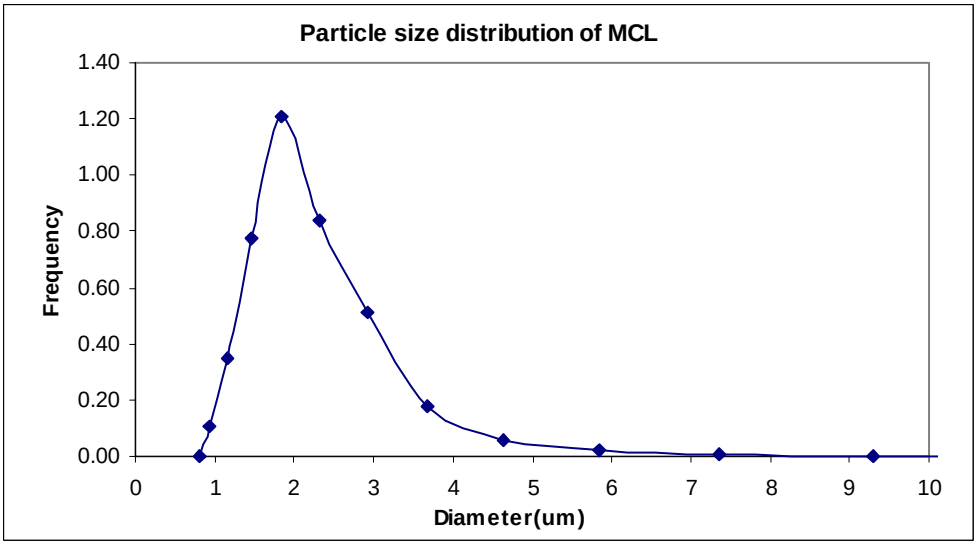

Figure 4.1 Particle size distribution of micronized lactose

Figure 4.2 depicts the accumulative particle size distribution of MCL. Over ninety percent of the particles fall on the range smaller than 5 µm as expected.

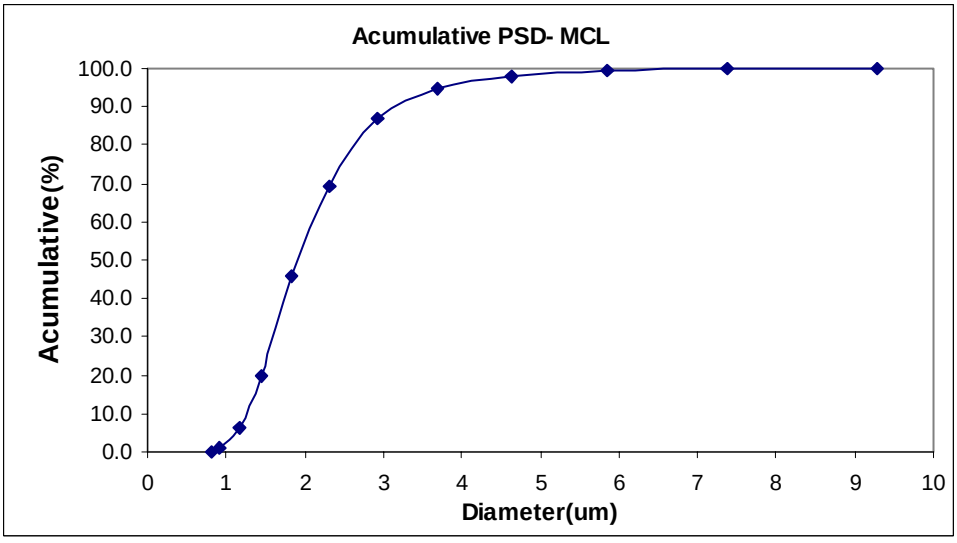

Figure 4.2 Particle size accumulative of micronized lactose

4.2.2 Analysis of Micronized Lactose with SEM

The MCL particles were sampled at different magnifications, from X1600 – X5500. At X1600, the particles are observed to be agglomerated, but their morphology cannot be determined at that magnification set up. However, at X5500, agglomeration of the particles is observed, and the morphology of the particles is well defined.

The MCL particles in the image are smooth in the surface, texture, and spherical shape. There is no unshaped particle. The particle sizes are uniform.

Figure 4.3 shows the morphological structure of MCL.

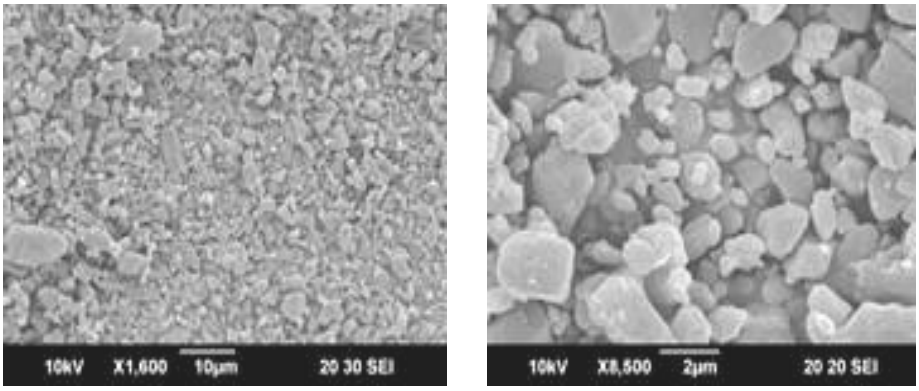

Figure 4.3 Morphology of MCL X1600 and X5500

4.2.3 Analysis of Micronized Lactose with FTIR

Figure 4.4 depicts the MCL IR Absorbance spectrum. The highest absorbance occurs in the wavenumber region between 989 – 1144 cm^{-1}. The MCL lowest absorbance occurs in the wavenumber region of 850 – 970 cm^{-1}. The group's frequencies for carbon-hydrogen, carbon-carbon, carbon-oxygen, and hydrogen-oxygen bonds can be found in the wavenumber region of 780 – 1680 cm^{-1} [55].

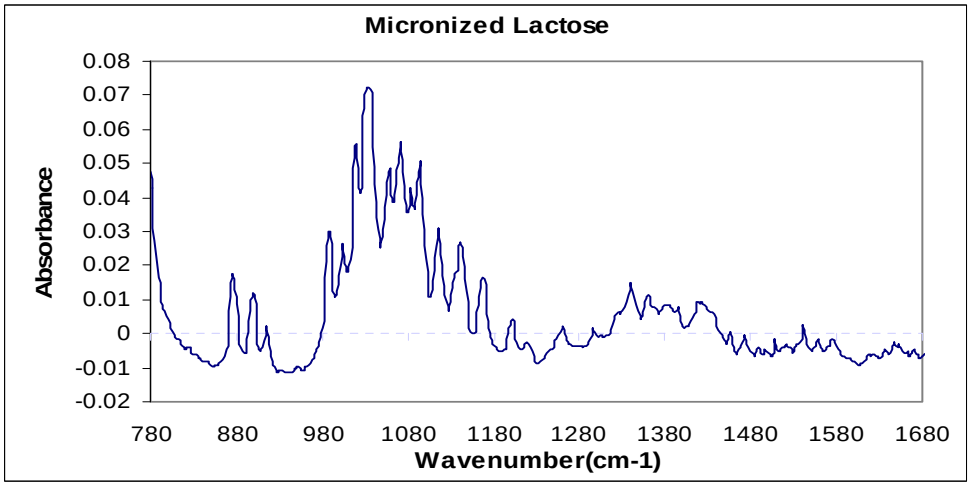

Figure 4.4 FTIR spectrum of micronized lactose

4.2.4 Analysis of Micronized Lactose with XRD

Figure 4.5 depicts the XRD Diffractogram of MCL. As can be seen, MCL shows the highest intensity at 20°. In this zone there is a greater concentration of atoms. At 13°, 17°, 21°, and 24°, MCL shows similar intensities; which confirm similar crystalline structures. The micronized lactose has a monoclinic arrangement. The intensity of the peak has a direct relationship with atoms concentration.

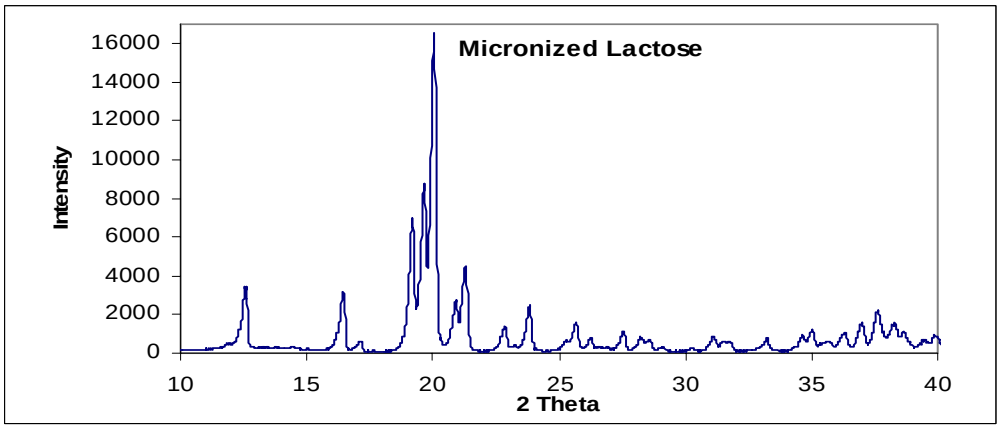

Figure 4.5 XRD of micronized lactose

4.3 Crystallization Process of Naproxen Sodium

Naproxen sodium solution was sprayed through the nozzle at high vacuum pressure to precipitate crystalline naproxen sodium (CNS) to reduce the particle size. Different trials that were performed at the fluid bed processing unit manipulating the operating parameters until the optimum conditions were acquired. The manipulated operating parameters were the fluidization speed, the concentration of the active ingredient solution, temperature, pressure, the aspersion flow, and the drying time. The experimental results obtained:

Figure 4. 6 depicts the particles obtained from the solution NS-water at different concentrations. As can be seen the crystallization generates agglomeration.

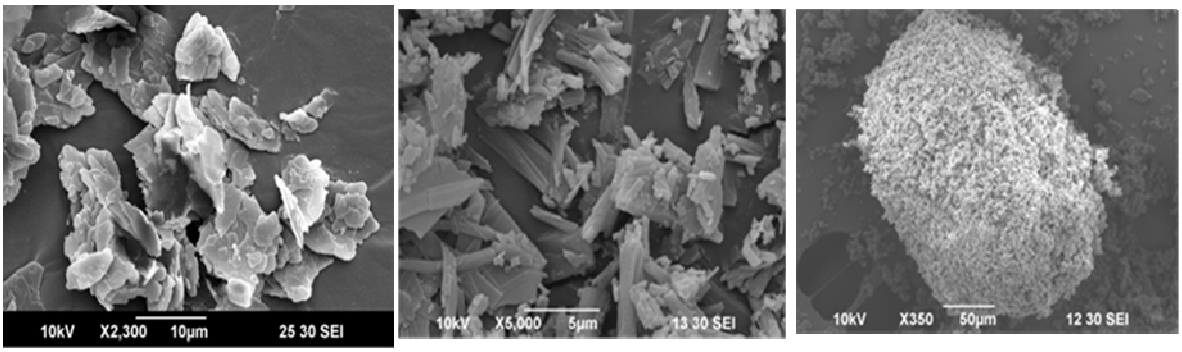

Figure 4.6 Crystallized naproxen sodium using water

To avoid the agglomeration a solution with ethanol and water was prepared at different concentrations. The ethanol solution was used to lower the surface tension to reduce the agglomeration of the particles in the FBD. Tests were carried out using different concentration of ethanol; the analysis with the SEM was possible to determine the conditions that produce the least agglomeration. Figure 4.7 depicts crystallization using solvent ethanol.

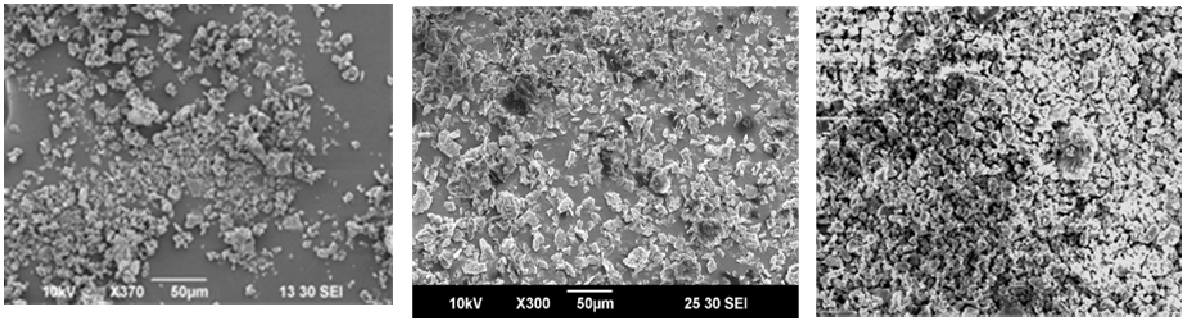

Figure 4.7 Crystallized naproxen sodium using ethanol

The optimum concentration obtained with the SEM was the 30 % v/v ethanol solution. The process the determine the adequate NS percent by weight included the precipitation from these solutions, and analysis of the particles with the SEM. The optimum percentage obtained was 20 % w/w. At higher percentages the solution is saturated, and at low percentages no significant crystals are formed. In addition, the pressure is manipulated until the optimum pressure is obtained at 551.43 kPa (80 psig), because the particle sizes were less than 5 µm. At lower pressure, the particle sizes obtained are above the 5µm, and the pressure can not be set above the 80 psig due to the equipment capabilities. When the equipment is set at higher pressure produce particles less than 5 µm.

The temperature was maintained constant at 313.15 K. The temperature is obtained by testing several temperature settings, and it is observed that at lower temperature the formation of crystalline strings occur. However, at higher temperature the ethanol solution vaporized. The alcohol content is reduced, thus agglomeration occurs again.

4.3.1 Particle size Distribution of Naproxen Sodium Crystallized

The particle size distribution is shown in Figure 4.8. The average particle size is 2.28 µm, and standard deviation 1.53, using the (SEM).

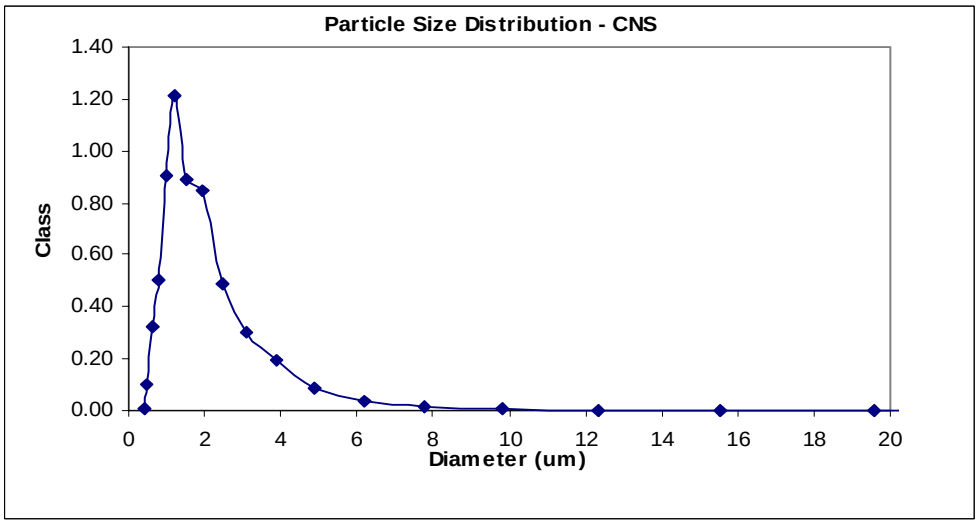

Figure 4.8 Particle size distribution of Naproxen sodium crystallized

Figure 4.9 shows the accumulative particle size distribution of naproxen sodium crystallized. As can be seen, 90% of particle sizes are below of 5 µm.

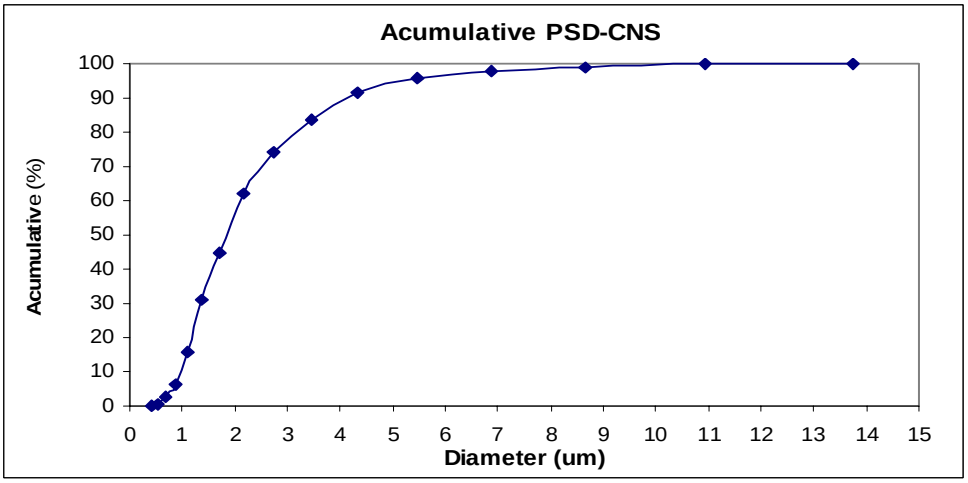

Figure 4.9 Particle size accumulative of Naproxen sodium crystallized

4.3.2 Comparison of CNS and NS, FTIR Absorbance

The spectra obtained in FTIR for CNS and NS were for the wavenumber regions of 780-1680 cm^{-1} region. It is observed that both spectra are similar, which confirms that the functional groups in CNS and NS are equivalents. The greater absorbance is caused by the higher atoms concentration in CNS in comparison with the NS which absorbance is less. Figure 4.10 showed the spectra of CNS and NS.

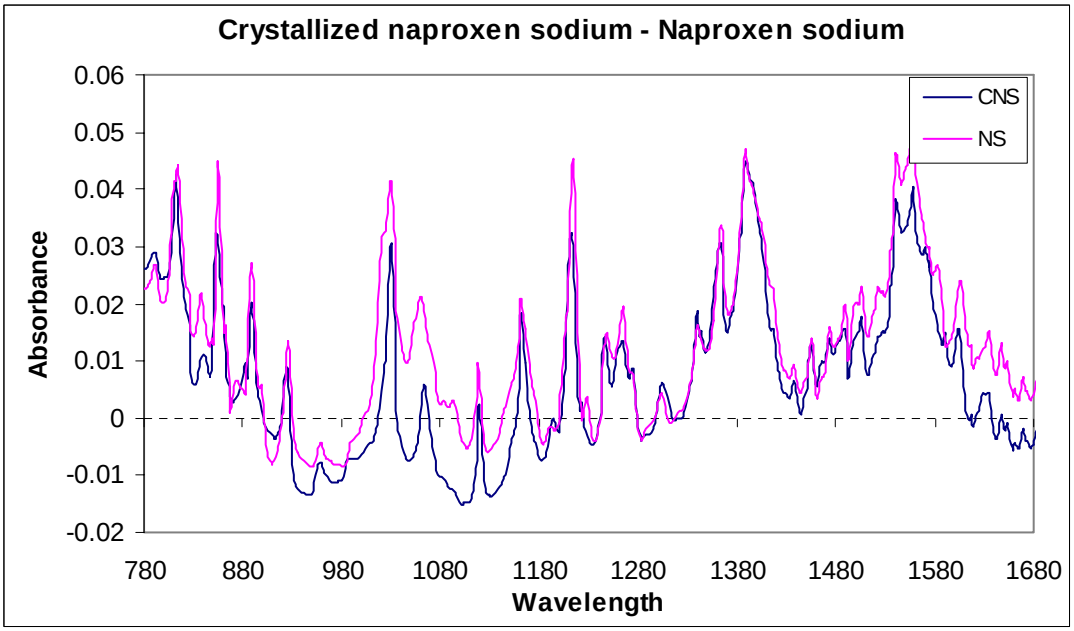

Figure 4.10 FTIR spectra of naproxen sodium original and crystallized naproxen sodium

Figure 4.10 demonstrates FTIR patterns for NS. Naproxen sodium exhibits sharp bands at 1200 cm^{-1} due to C-O-stretching (ether), 1250 cm^{-1} due to C-O-stretching (acid)

1390 to 1360 cm^{-1}due to CH_3 bending, 1480 cm^{-1} due to asymmetrical COO- stretching, 1580 cm^{-1} due to symmetrical COO-stretching, 1628 cm^{-1} due to C-C aromatic skeletal stretching [50].

4.3.3 Comparison of CNS and NS by XRD

X-ray diffraction is a proven tool to study crystal lattice arrangements and yields very useful information on degree of sample crystallinity. XRD patterns of CNS and NS were obtained over a diffraction-angle (2θ) range of 4 to 80°, with a step size of 0.02 º, and a counting time of 1.0 second per step. Figure 4.11 shows the diffractogram of the CNS and NS.

The XRD scans shows significant variations between samples, since the difference on the intensity is due to the lattice movements which are farther when the crystallization occurred. The scanning range was selected to show the areas of interest, mainly the main naproxen sodium peak and peaks for NS and CNS, with enough range extending either side to give a picture of the amorphous diffractogram. At the 14–18° angle the NS and CNS have higher intensity. At the 22 - 42° angle there is no significant differences on the intensities because they have similar crystalline structure.

As is evident from Figure 4.11 marked more less differences in the CNS and NS were observed. Sharp peaks were noted in the diffraction pattern of NS at 2θ values of 15, 19, and 26. See Appendix D.

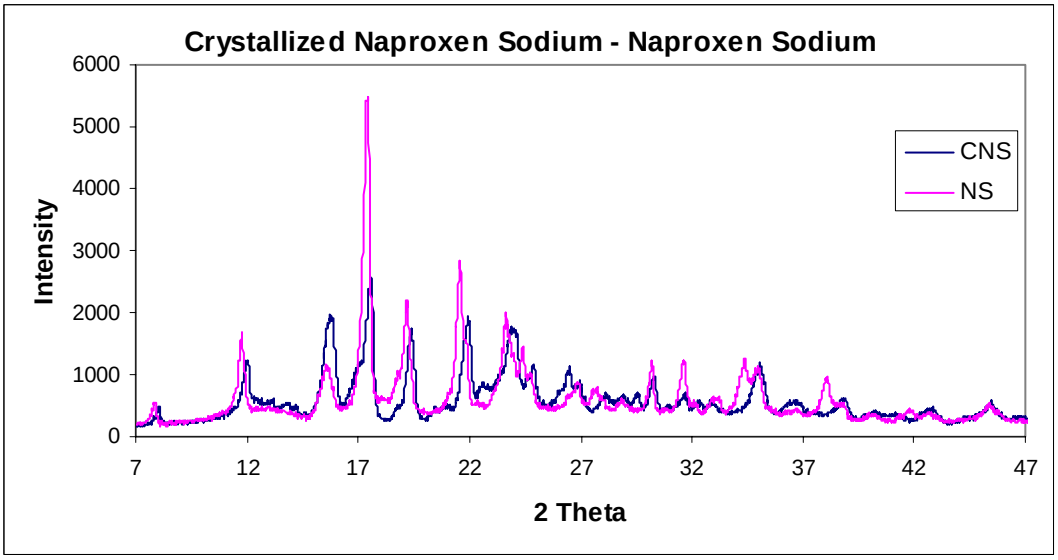

Figure 4.11 XRD of Naproxen sodium original and crystallized naproxen sodium in fluid bed dry at 40°C and 80 psia

The XRD diffractogram show diffraction of polymorphic and pseudo polymorphic forms. This clearly demonstrates the differences in the lattice structures. The both the anhydrous and the monohydrated crystals of naproxen sodium crystallize can be observed in the space group.

The particle size of the crystalline naproxen sodium analysis can be obtained with the Scherrer Formula.

$$t = \frac{K\lambda}{B\cos\theta_B} \qquad (4.1)$$

Where *t* thickness of crystallite, *K* constant dependent on crystallite shape (0.89), *l* x-ray wavenumber, *B* FWHM (full width at half max) or integral breadth, and q_B Bragg Angle.

For naproxen sodium in the range: 17.24° - 17.54°, where θ is 0.30°, 2θ is 17.58° crystal size 0.982μm, and crystallized naproxen sodium in the range 17.64° - 17.02°, where θ is 0.63°, 2θ is 17.58° crystal size 0.471μm. Therefore reduce size by crystallization process.

	Angle (2θ)	**Size (t)**
Naproxen sodium	17.58	0.982 μm
Naproxen sodium crystallized	17.58	0.471 μm

Table 4.3 Reduction of naproxen sodium

4.4 Particle Adhesion for Functionalization

The operating conditions used during the particle functionalization were the ones used during the crystallization process. The only difference performed during the particles functionalization was to feed MCL first to the fluid bed processing unit chamber. Once, the fluidization started the solution of the active ingredient was then added.

The FP have different morphologic forms; due to particles adhesion of the CNS over MCL. The adhesion between the particles is due to the impact forces with other particles. They can be formed at diverse impact forces when they are in contact with the particles; the diverse forces that coexist are normal forces, central impact forces, tangential forces, torsion forces, and moment forces.

4.4.1 Formation of Functionalized Particles

The functionalized particle (FP) is formed by the particle adhesion caused by surface and field forces. Van der Waals forces prevail, the intermolecular forces, electrostatic forces, magnetic forces, and vibration forces causes the material to form bridges between the particle surfaces solution and LMC as part of the fluid bed processing [31].

The material formed bridges between the particle surfaces; in addition hydrogen bonds of adsorbed surface layers of condensed water (powders) are formed; and organic macromolecules formed flocculants in suspensions.

The liquid bridges are formed by low viscous wetting liquids, the capillary pressure, and surface tension is very low.

4.4.2 Particle Size Distribution of Particle Functionalized

In the final process, samples are taken from the dried material to be analyzed on the SEM. This is done to determine the size of the particles and the morphology. The particles are distributed throughout the all surfaces, and the average diameter of the particles is 4.04 μm, with an standard deviation of 2.481.

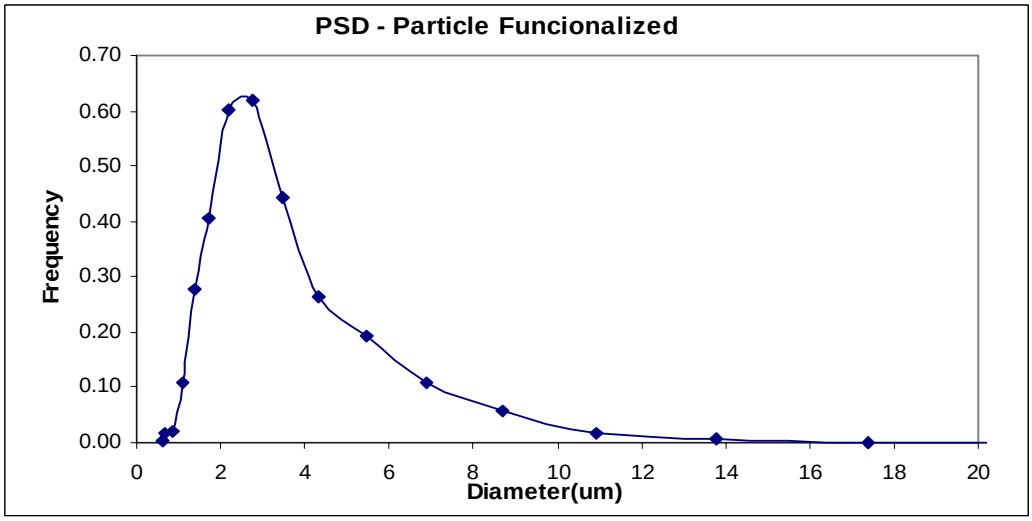

Figure 4.12 Particle size distribution of particles functionalized

The accumulative particle sizes are shown in the Figure 4.13. In this case, it was observed that 70% of particle sizes are lower than 5 μm.

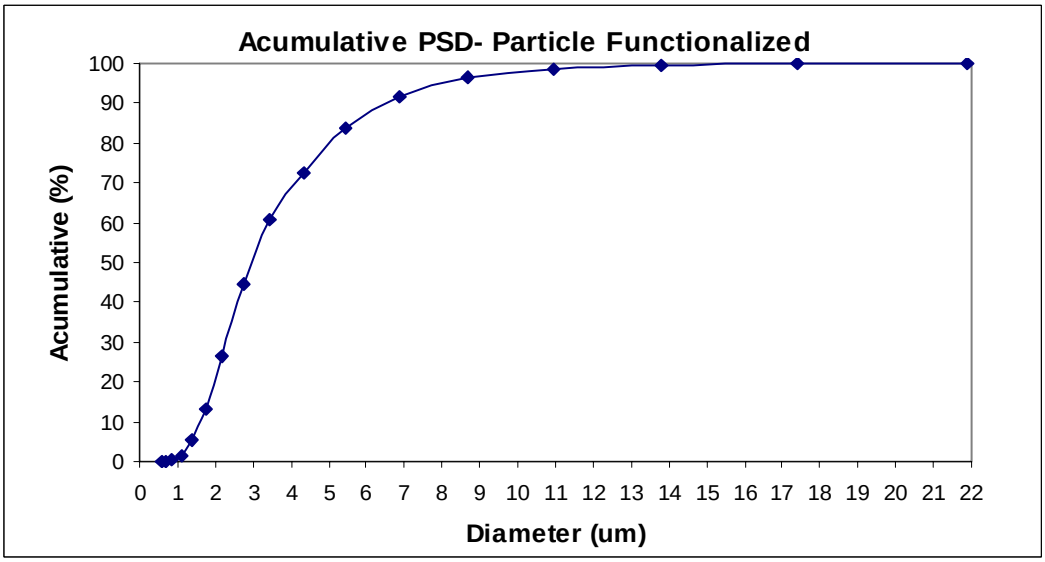

Figure 4.13 Accumulative particle size of material functionalized.

4.4.3 Analysis Particle Functionalized (FP) by SEM

Figure 4.14, shows the particles functionalized which confirm the adhesion of small particles averaging less than 1.0 µm to large particles averaging around 5 µm. The identification of the small particles was performed using SEM. The average size is 4.040 µm. See Appendix A.3 to A.6.

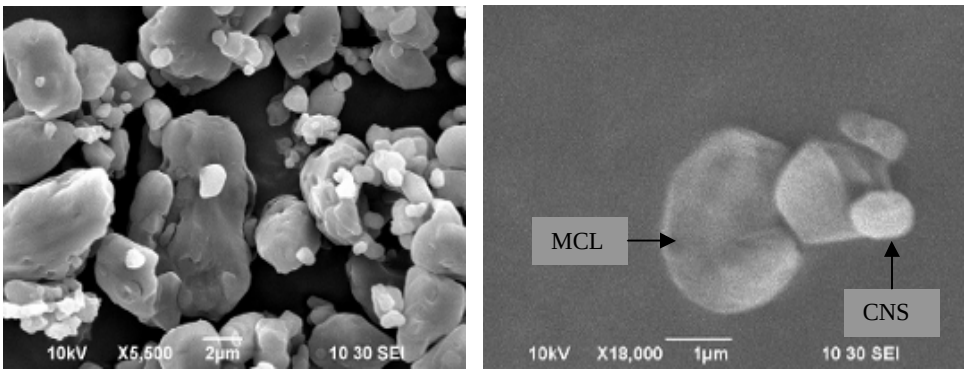

Figure 4.14 (a) Image of FP of CNS on MCL with magnification X5000 and

4.4.4 Analysis Particle Functionalized (PF) by EDAX

The EDAX identifies the quantity of the sodium element in the particles functionalized. The quantitative analysis demonstrated that 2.39% were sodium. Figure 4.15 illustrated this process. See Appendix C.

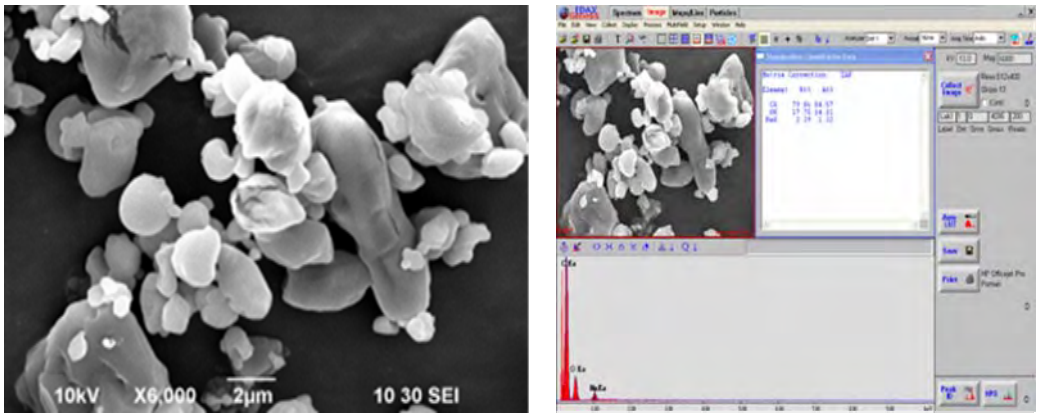

Figure 4.15 EDAX Analysis of particles functionalized

4.4.5 Analysis of Particles Functionalized (PF) by Fourier Transformed Infrared (FTIR) Spectroscopy

Figure 4.16 depicts the FTIR spectra for 4 samples of the particles functionalized. On the wavenumber region of 700-1000 cm^{-1} the characteristic peaks were obtained, and can be demonstrated that the spectra are displaced in such a way that the entire spectrum did not fall at the same peak. While at the regions 1000-1100 cm^{-1}, the entire spectra show the same characteristic peaks. The characteristic peaks determine the chemical properties of the functionalized material.

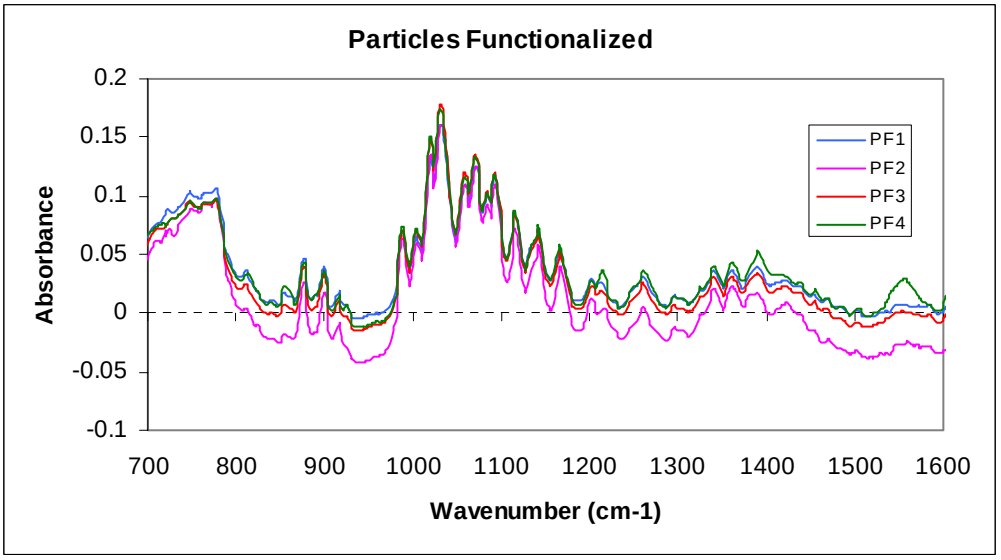

Figure 4.16 FTIR of functionalized between crystallized naproxen sodium on micronized lactose in fluid bed dry at 40°C and 80 psia

Figure 2.17 depicts the comparison of the FTIR spectra of functionalized particles (FP) suggested that all the studied FP samples processed into the α- lactose and β-lactose. In an attempt quantify these changes, the ratio of the absorbance at 980 cm^{-1} for lactose, believed to be associated mostly with ring C-C-stretching vibrations, to that at 1030 cm^{-1}, believed to result from C-O-stretching vibration of the CH_2-OH (as the other C-O-stretching vibrations, such as the ring CH-O and C-O, would be expected to contribute at higher wavenumber) was calculated [50].

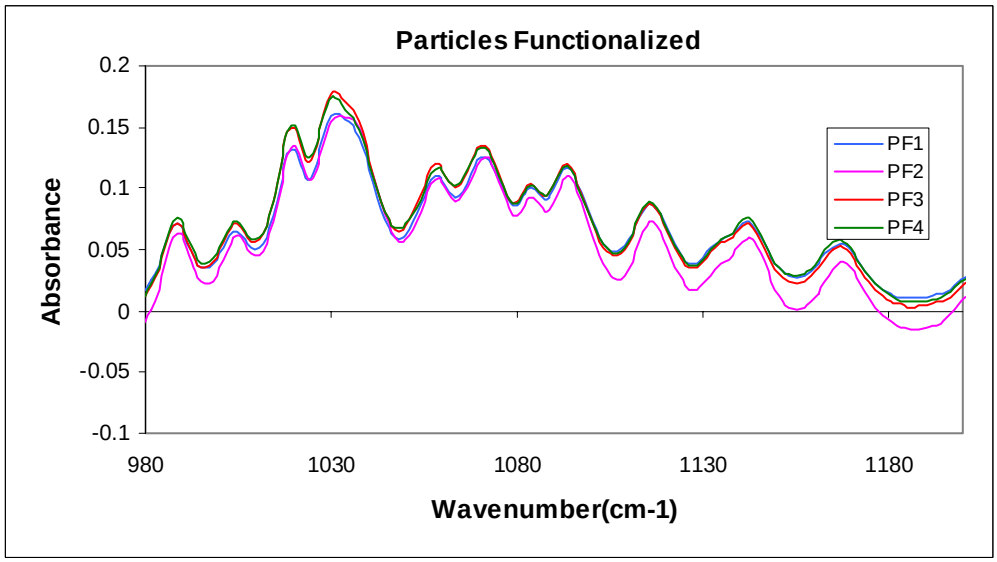

Figure 4.17 FTIR spectra of particles functionalized 980-1200 cm^{-1}

Figure 4.17 depicts the wavenumber region of 980-1180 cm^{-1} the characteristic peaks were obtained, and can be demonstrated that the spectrums are similarity. The spectra observed are similar. It owes himself that there is not change of functional groups [50].

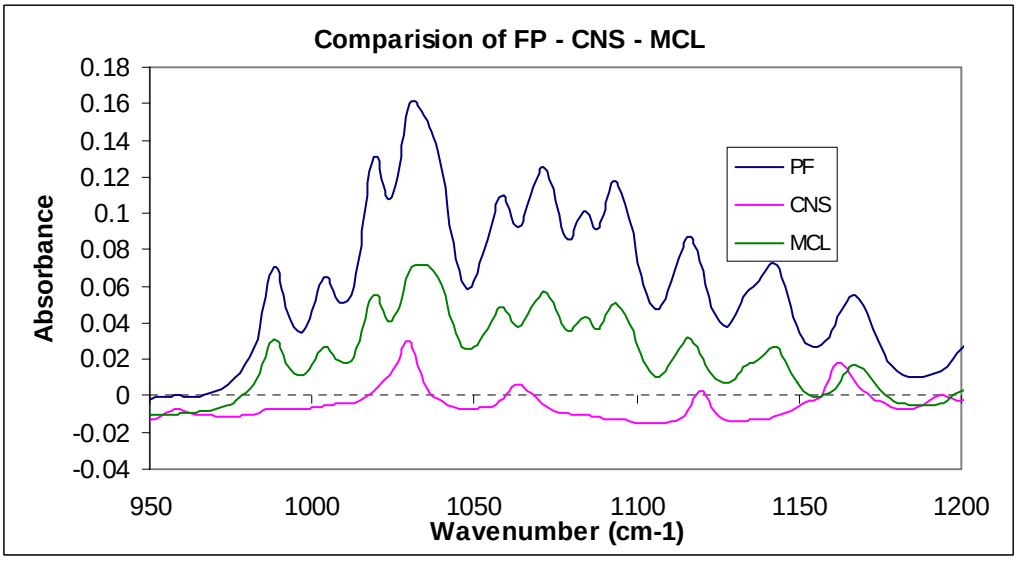

Figure 4.18 FTIR comparison between FP, CNS, and MCL.

Figure 4.18 depicts bigger absorbance of the functionalized particle, followed by lactose micronized. The one that has smaller absorbance is the CNS.

4.4.6 Analysis of Particles Functionalized (PF) by XRD

Knowing the crystallized structure is very important to help identifying the physical and chemical properties.

The particle size of the crystalline FP and CNS analysis can be obtained with the Scherrer Formula.

$$t = \frac{0.89\lambda}{B\cos\theta_B} \qquad (4.2)$$

Where *t* thickness of crystallite, *K* constant dependent on crystallite shape (0.89), *l* x-ray wavenumber, *B* FWHM (full width at half max) or integral breadth, and q_B Bragg Angle.

For functionalized particle in the range: 20.00° - 19.72°, where θ is 0.28°, θ is 19.90° crystal size average 1.016 µm, the concentration is remained constant and crystalline structure is very compact. In the present study, XRD technique was used to identify and confirm the crystal forms of functionalized particle components after crystallization. Characteristic peaks for α-lactose were observed at 12.5° and 16.4°, whereas the characteristic peak for β-lactose.

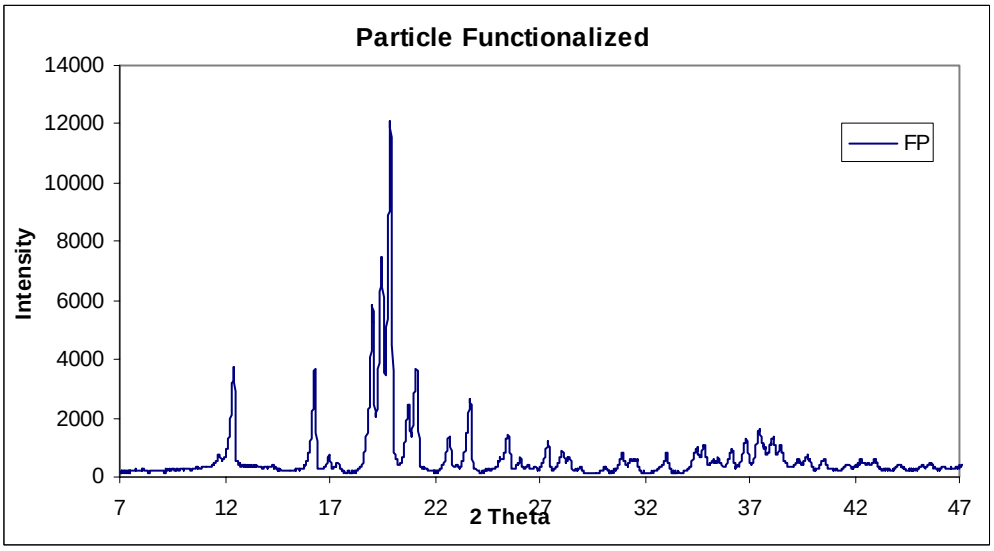

Figure 4.19 XRD of particle functionalized

4.4.7 Comparison between CNS, NS, and FP by XRD

Figure 4.20 depicts MCL with higher intensity, while the material functionalized (MF) has smaller intensity; this is causes because the CNS covered the MCL; therefore the

adsorption capacity is less. In some regions it can observed that the CNS is adhered to the particles of MCL.

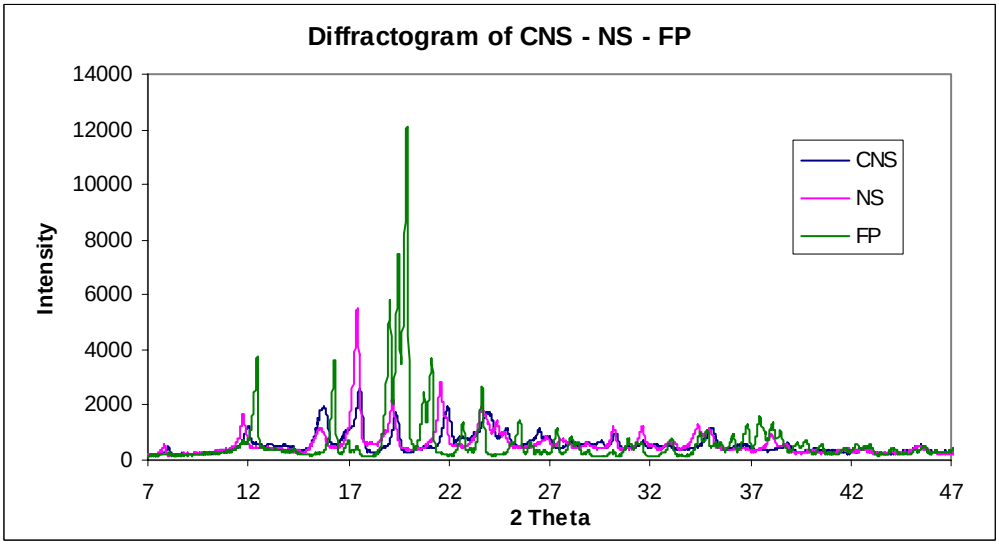

Figure 4.20 XRD of CNS, NS, and FP

Comparing the scans of MCL and FP in Figure 4.20, it appears that there is less crystalline content in the MCL conditions, since the particular isomer of lactose cannot be distinguished and, although the main peak is visible, the peak counts are visibly lower than those of the FP. For the MCL the main peak is approximately 20° while the FP peak is approximately 19.9°.

In general there is no change in the crystalline structure of MCL and FP. The crystalline structure both cases maintain equal, because very important for use as inhaler powder.

4.4.8 Statistical Analysis of Functionalized Particle

The analysis of variance (ANOVA) [18] experiment was developed with all the experimental data gathered, and it was found that the F- value obtained is 18.18, and P is 0.005. This implies that the model is significant for absorbance, R^2 is 75.19%. The confidence level is 95% and, the value of α is 5%. Therefore implies the model is significant. There is only a 0.50% chance that a "Model F- Value". See Appendix E.

The average particle size of lactose micronized is 2.34 µm with a standard deviation of 0.97. The average particle size of crystallized naproxen sodium is 2.28 µm with a standard deviation of 1.53. The average particle size of functionalized particle is 4.04 µm with a standard deviation of 2.48.

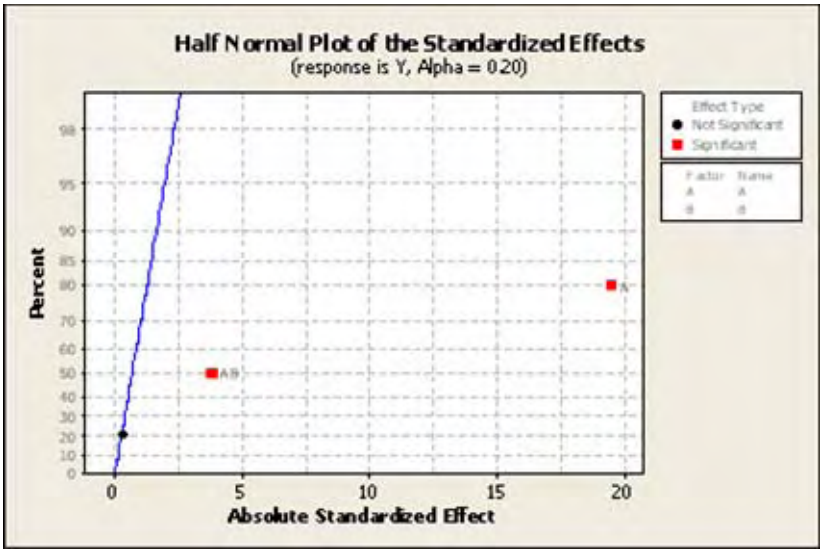

Figure 4.21 Residual Half Normal

Residual plot of experiment the Figure 4.21 shown the residual plot the don't show any important parameter, any considerable deviation doesn't exist in funcionalization particles.

There is nothing unusual about the residual plots; therefore, the analysis of variance assumptions are satisfied. Very important the interaction pressure and temperature, the affect pressure, and temperature appear to be large process in the fluid bed dryer processing.

5 CONCLUSION AND RECOMMENDATION

The studies conduced indicate that:

The precipitation of particle of naproxen sodium with size less than 5 μm by crystallization in fluid bed dryer process at high vacuum pressure were obtained

The functionalized particles of crystallized naproxen sodium on lactose micronized in the fluid bed dryer process at high vacuum are achieved, due to the morphological, Van der Waals, electrostatic, and magnetic forces.

The average particle size of the functionalized material determined by the SEM was 4.04 μm with a standard deviation of 2.48. The particle size accumulative distribution falls 80 % underneath the 5 μm. The morphology of the particles tends to be spherical as the CNS has a tendency to adhere on MCL. The FTIR spectrum was shown between wavenumber 1000 - 1100 cm^{-1}, and an equivalent crystalline structure can be observed. In the region of 700 - 1000 cm^{-1} and 1100-1600 cm^{-1} a difference on the size can be observed.

The particle functionalized was analyzed using the XRD in the angle 2θ: 7° - 47°, where it shows greater intensity at the peaks underneath the characteristic zone. The crystalline structure of NS in its different polymorphic forms and new crystalline structure was observed.

The chemical properties of the transformed NS to CNS were analyzed with the FTIR spectroscopy. The optimal operating conditions obtained for the XRD using copper Kα

1.54056 A°, start at 7° and stop angle 47°, time step 1 second, step size 0.02°, scan continuously. The different spectrums and polymorph transformations of NS were observed. In addition, the CNS spectrums were displaced to the right side from the NS spectrums.

The particle functionalized can be used in the formulation of powder for inhalation fundamentally in pharmaceutical, and food industry.

Future Studies:

The study of the functionalized particles prepared in a fluid bed processing unit is highly recommended to obtain more knowledge and different operating conditions can be obtained. The use other active ingredients is recommended. This will provide more information about the behavior of the active ingredient as a key component to the functionalized particles.

REFERENCES

[1] K. Källander, et al. 2008. *Bulletin of the World Health Organization* Volume 86, Number 5, 321-416.

[2] A. Muñoz. 2006. Inhaladores de polvo seco para el tratamiento de las enfermedades respiratorias: Parte I. *Rev Cubana Farm*, vol.40, Nro.2, p.0-0. ISSN 0034-7515.

[3] A. Muñoz 2006. Adriana. Inhaladores de polvo seco para el tratamiento de las enfermedades respiratorias: Parte II. *Rev Cubana Farm*, vol.40, Nro. 2, p.0-0. ISSN 0034-7515.

[4] S. Alavi and B. Caussat. 2005. Experimental study on fluidization of micronic powders, Powder Technology Volume 157, Issues 1-3, 4th French Meeting on *Powder Science and Technology*, Pages 114-120.

[5] D. Kunii and O. Levesnpiel. 1991. Fluidization Engineering, Butterworth-Heinemann series *in Chemical Engineering*.

[6] E. Teunou and D. Poncelet. 2002. Batch and continuous fluid bed coating - review and state of the art, *Journal of Food Engineering* Volume 53, Issue 4, Pages 325-340

[7] US. Department of Health and Human Services. 1998. Food and Drug Administration, Center for Drug Evaluation and Research (CDER). Drug Products Chemistry, Manufacturing and Controls Documentation. *Document* 2180. Rockville. FDA.

[8] G. Bruni, et al. 2007. An investigation of the effect of the inter-particle forces on the fluidization behaviour of fine powders linked with rheological studies, *Chemical Engineering Science* Volume 62, Issues 1-2, Fluidized Bed Applications, Pages 387-396.

[9] L. Huilin, D. Gidaspow and J. Bouillard. 2002. Chaotic behavior of local temperature fluctuations in a laboratory-scale circulating fluidized bed, *Powder Technology* Volume 123, Issue 1, Pages 59-68.

[10] J.F. Richarson, J.F. Davidson and H. Harrison. 1971. Fluidization eds., *Academic Press,* New York. Page 1-26.

[11] S.C. Saxena and G.J. Vogel. 1977. *Trans. Int. Chem. Eng*., 55, 184 *Chem. Eng. J*., 14, 59 .

[12] S.P. Badu, B. Shah, and A. Talwalkar. 1978. *AIChE symp. Ser*.,74(176), 176

[13] J.R. Grace. 1982. Hambook of Muliphase Systems, G. Hertsroni, ed., *Hemisphere*, Washington, D.C. p. 8-15

[14] D.C. Chistester et al. 1985 *Chem Eng. Sci*., 39, 253.

[15] S. Watano, et al. 2003. Microgranulation of fine powders by a novel rotating fluidized bed granulator, *Powder Technology* Volume 131, Issues 2-3, Pages 250-255.

[16] W. L. McCabe, et al. 1993. Unit Operations of Chemical Engineering. *McGraw-Hill*, Inc. page 767 – 923.

[17] F. Liang – Shih, et al. 1998. Principles of Gas- Solid Flows. *Cambridge Series in Chemical Engineering* page 3-543.

[18] C. D. Montgomery. 2005. Design Analysis of Experiments. *McGraw-Hill*, Inc page 60-122.

[19] E. Rivera. 2004 Optimization of Drying-End-Points Measurements for the Automation of a Fluidized-Bed Dryer Using FT-NIR Spectroscopy. Master thesis *Chem. Eng.* UPRM.

[20] Y. Wen-Ching Yang. 1998. Siemens Westinghouse *Power Corporation Pittsburgh*, Pennsylvania. USA.

[21] L.S. Fan. 1989. *Gas- Liquid – Solid Fluidization Engineering*, Butterworth-Heinemann *series in Chemical Engineering*.

[22] S. Rodríguez-Rojo, et al. 2007. Residence time distribution studies of high pressure fluidized bed of microparticles, *The Journal of Supercritical Fluids In Press*, Corrected Proof, Available online.

[23] R.L. Stephen, et al. 2007. Air-suspension particle coating in the food industry: Part I: state of the art, *Powder Technology* Volume 171, Issue 1, Pages 25-33.

[24] D. Geldart. 1973. Types of gas fluidization, *Powder Technology* Volume 7, Issue 5, Pages 285-292.

[25] D. Geldart and A. R. Abrahamsen. 1978. Homogeneous fluidization of fine powders using various gases and pressures, *Powder Technology* Volume 19, Issue 1, Pages 133-136.

[26] J. Tomas. 2007. Adhesion of ultrafine particles-A micromechanical approach, *Chemical Engineering Science* Volume 62, Issue 7, April 2007, Pages 1997-2010.

[27] D. Geldart, et al. 1986. Determination of the density of porous particles using very fine dense powders, *Powder Technology* Volume 45, Issue 2, Pages 173-176.

[28] D.M. Parikh. 1990. Fluid bed processing in the 1990's. GEA Niro Inc. article available at www.niroinc.com/pharmarticles/airflow.html, pp 1-9.

[29] A.B.Delebarre, et al. 1994. Fluidization and mixing of solids distributed in size and density. *Powder Technology* Volume 80: 227-233.

[30] R.E. Treybal. 1980. Mass transfer operations. Published by the *McGraw Hill Company*, Inc., NY, USA, pp.655-686.

[31] D. Maugis, 1999. Contact, Adhesion and Rupture of Elastic Solids. *Springer*, Berlin

[32] J.N. Israelachvili, 1992. Intermolecular and Surface Forces. *Academic Press*, London

[33] K.L. Johnson, A.D. Roberts, 1971. Surface energy and the contact of elastic solids. *Proceedings of Royal Society* A 324, 301–313.

[34] W.J. Stronge, 2000. Impact Mechanics. Cambridge University, *Cambridge*. pp. 116–126.

[35] W.K. Li., E.G. Karpov, H.S. Park, 2006. Nano Mechanics and Materials: Theory, Multiscale Methods and Applications. *Wiley, Chichester*.

[36] J. Tomas., 2000. Particle adhesion fundamentals and bulk powder consolidation. KONA - *Powder and Particle* Volume 18, 157–169.

[37] M. Van Oort. 1995. In vitro testing of dry powder inhaler. *Aer Sci Technol*. 1995;22:364-73

[38] J.M. Montenegro. 2001. Modeling and Automation of a Fluid Bed Dryer for Determination of Optimum Drying End Points of Pharmaceutical Granulations. Master thesis. *Chemical Engineering*. UPRM.

[39] F.E. Milioli and P.J. Foster. 1995. A model for particle size distribution and elutriation in fluidized beds, *Powder Technology* Volume 83, Issue 3, Pages 265-280.

[40] K. Young-Soo, 2005. Crystallization And Solid-State Transformation Of Pseudopolymorphic Forms Of Sodium Naproxen. Ph.D Thesis *Georgia Institute of Technology*. USA.

[41] D. Geldart and A.C.Y. Wong. 1984. Fluidization of powders showing degrees of cohesiveness--I. Bed expansion, *Chemical Engineering Science* Volume 39, Issue 10, Pages 1481-1488.

[42] D. Geldart. 1972. The effect of particle size and size distribution on the behaviour of gas-fluidised beds, *Powder Technology* Volume 6, Issue 4, Pages 201-215

[43] Y. Mawatari, T. Koide, Y. Tatemoto, S. Uchida and K. Noda. 2002. Effect of particle diameter on fluidization under vibration, *Powder Technology* Volume 123, Issue 1, Pages 69-74.

[44] S. Brandani and K. Zhang. 2006. A new model for the prediction of the behaviour of fluidized beds, *Powder Technology* Volume 163, Issues 1-2, Fluidization and Fluid Particle Systems, Pages 80-87.

[45] A. Walewijk, J.J. Cooper-White and D.E. Dunstan. 2008. Adhesion measurements between alginate gel surfaces via texture analysis, *Food Hydrocolloids* Volume 22, Issue 1 8th International Hydrocolloids Conference, Pages 91-96

[46] R.K. Singh, G.K. Roy. 2005. Prediction of minimum bubbling velocity, fluidization index and range of particulate fluidization for gas-solid fluidization in cylindrical and non-cylindrical beds, *Powder Technology* Volume 159, Issue 3, Pages 168-172.

[47] F. Podczeck. 2007. Particle-Particle Adhesion in Pharmaceutical Powder Handling. *Imperial College Press*. ISBN 1-86094-112-5. Pages 1-75.

[48] D. Chiou, T.A.G. Langrish. 2008. A comparison of crystallisation approaches in spray drying, *Journal of Food Engineering* Volume 88, Issue 2, Pages 177-185.

[49] MSDS. 2006. Number: L1131 *Effective Date:* January 16th, page

[50] B. Smith. 1999. Infra-Red Spectral Interpretation. *A systematic Approach*, CRC Press.

APPENDIX A. GALLERY PHOTOGRAPHY OF EXPERIMENTS

Figure A.1 Equipment Fluid Bed Dryer

Figure A.2 Experimental sample of lactose micronized

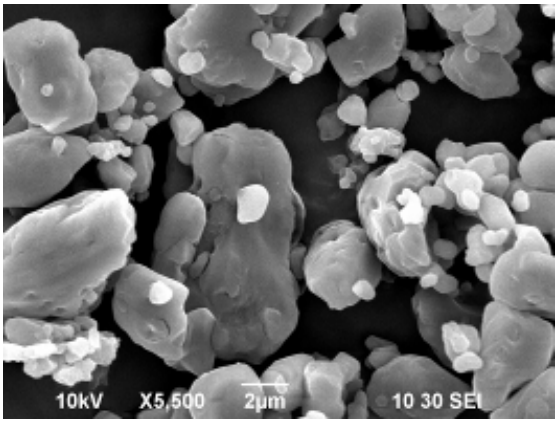

Figure A.3 Functionalized particle with water an ethanol

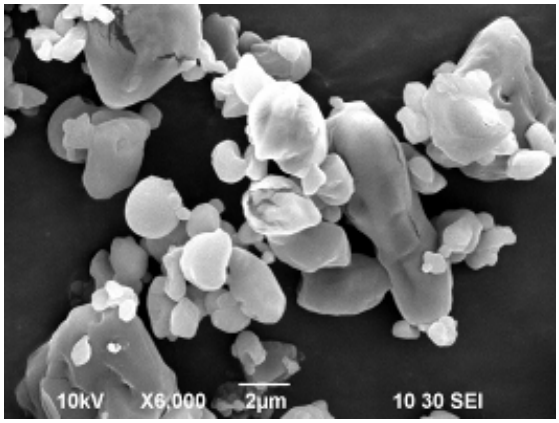

Figure A.4 Functionalized particle with water and ethanol

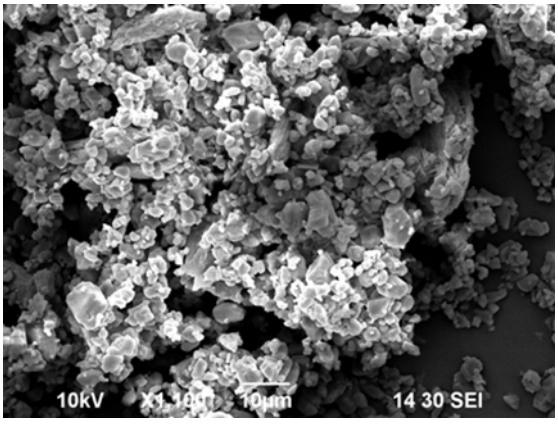

Figure A.5 Functionalized particle with water

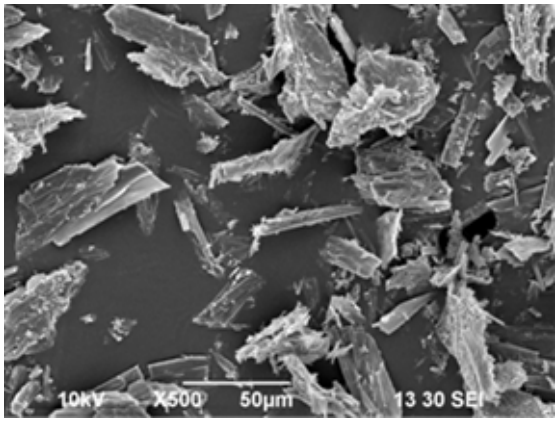

Figure A.6 Naproxen sodium original sample

APPENDIX B. CALCULATION OF SODIUM

NAPROXEN SODIUM SOLUTION		
Calibration flow		
Peristaltic Pump	**Unit**	0.75
Time	s	60
Volume	mL	60
Flow of pump	mL/s	1.00
Calculate theoretical of Naproxen sodium		
Mass MCL001	g	10.00
Aspersion time on fluid bed	s	30.00
Volume of solution	mL	32.50
Solution density	g/mL	0.99
Solution mass	g	32.29
Percentage in weigh (%W)		20.00
Mass Naproxen sodium	g	6.46
Weigh Molecule Naproxen Sodium	g/mol	252.24
Weigh atomic sodium	g/mol	22.99
Percentage sodium (%Na)		9.12
Mass Total	g	16.46
Weigh sodium	g	0.59
Percentage sodium theoretical (%Na)		3.58
Percentage naproxen sodium (%Naproxen)		39.24

APPENDIX C. EDAX RESULTS

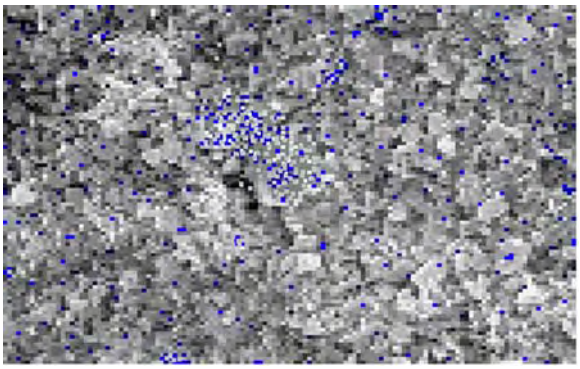

Figure C.1 Distribution naproxen sodium over lactose micronized. The color blue is NS

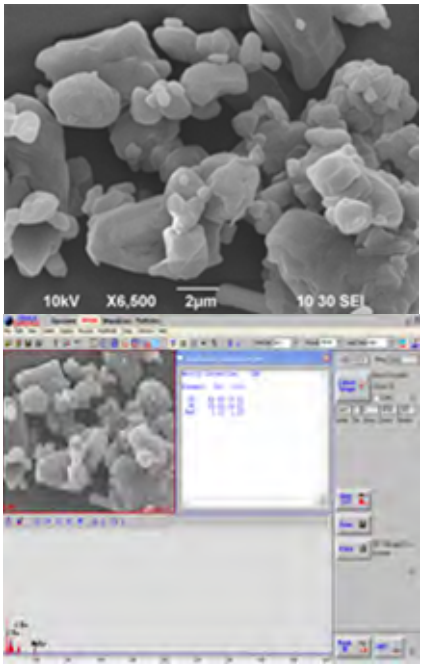

Figure C.2 EDAX analysis 2.39 % Sodium

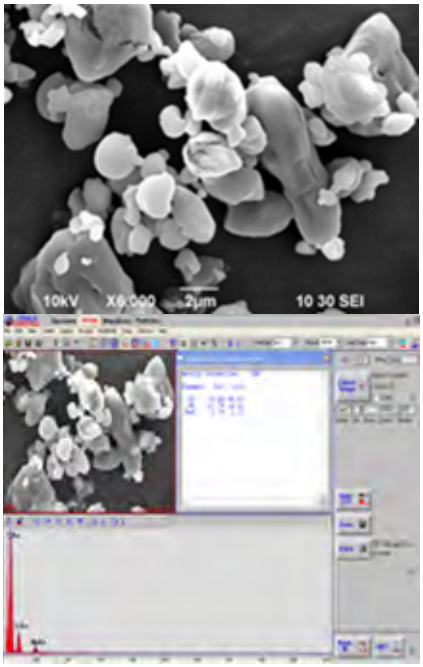

Figure C.3 EDAX analysis 3.49 % Sodium

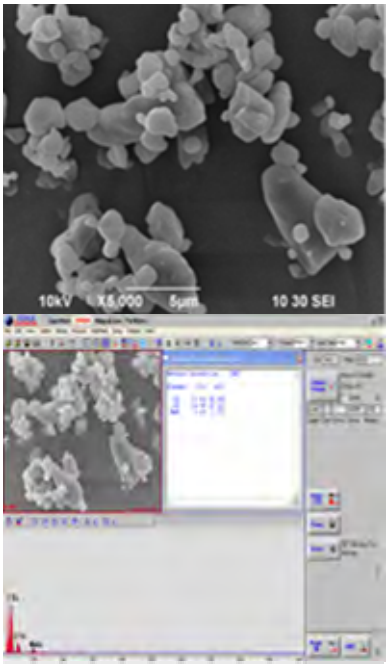

Figure C.2 EDAX analysis 3.23 % Sodium

APPENDIX D. XRD RESULTS

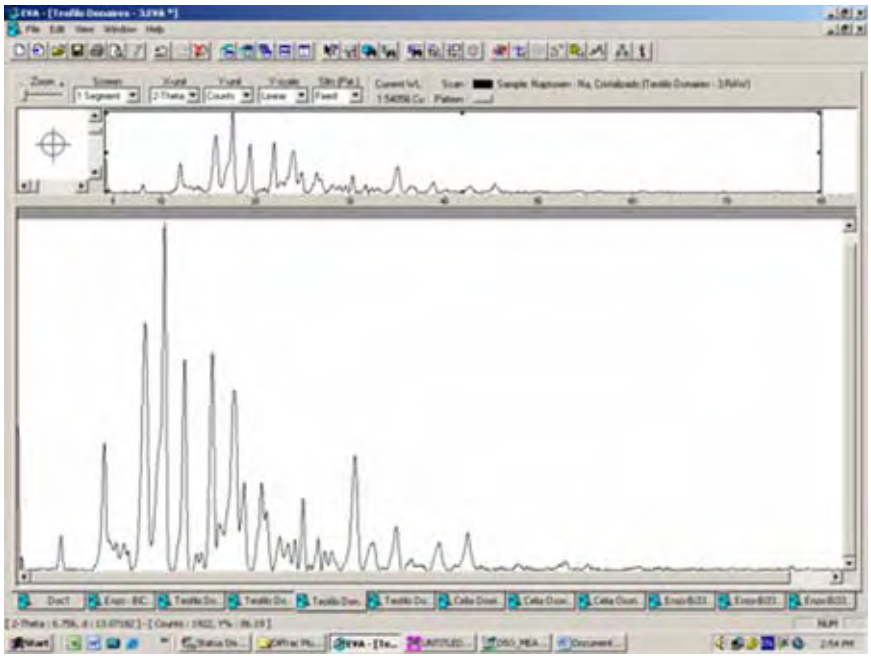

Figure D.1 XRD Analysis of Lactose Micronized

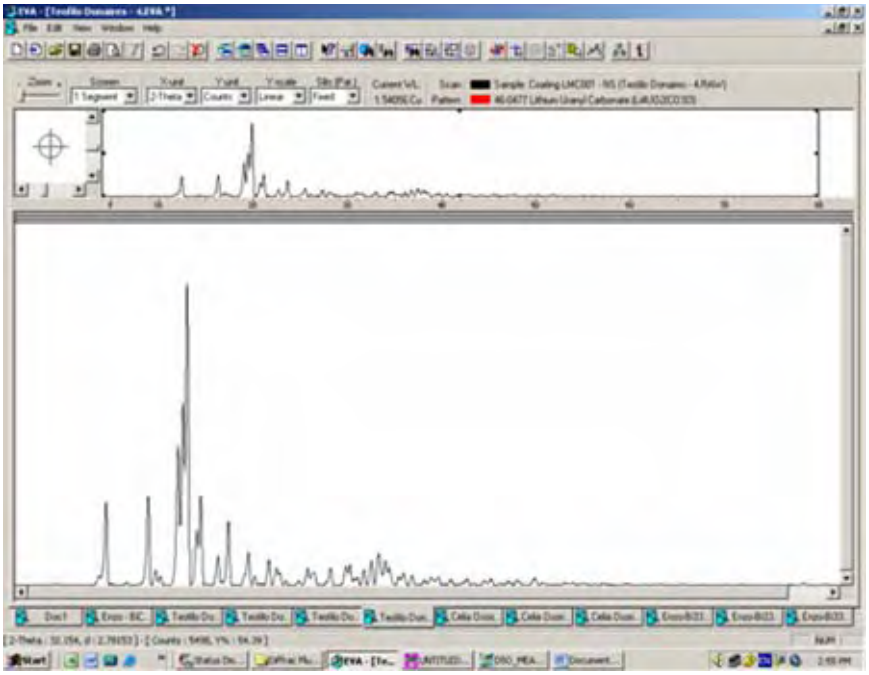

Figure D.2 XRD Analysis of Naproxen Sodium

APPENDIX E. OUTPUT MINITAB 15

One-way ANOVA: Response versus Treatment

```
Source     DF         SS         MS      F      P
Treatment   1  0.0015933  0.0015933  18.18  0.005
Error       6  0.0005257  0.0000876
Total       7  0.0021190

S = 0.009361   R-Sq = 75.19%   R-Sq(adj) = 71.05%


                           Individual 95% CIs For Mean Based on
                           Pooled StDev
Level  N     Mean    StDev  -----+---------+---------+---------+----
1      4  3.31942  0.00650  (-------*-------)
2      4  3.34765  0.01153                   (-------*------)
                           -----+---------+---------+---------+----
                              3.315     3.330     3.345     3.360

Pooled StDev = 0.00936
```